POLITECNICO
MILANO 1863

SCUOLA DI INGEGNERIA INDUSTRIALE
E DELL'INFORMAZIONE

Enhancing Gas Turbine Simulation for Hydrogen-Powered Aircraft

Master Thesis in
Energy Engineering - Ingegneria Energetica

Riccardo Di Loreto, 996664

Advisor:
Prof. Paolo Chiesa

Academic year:
2022-2023

Abstract: The expansion of global civil aviation and its significant carbon footprint necessitate innovative solutions aligned with environmental goals. Hydrogen, in conjunction with popular jet engines, emerges as an excellent candidate for achieving carbon-neutral flights, leveraging proven technology and potential performance improvements. Within the context of the European EFACA (Environmentally Friendly Aviation for All Classes of Aircraft) project, this research comprehensively analyzes a liquid hydrogen power system using a proprietary computer code from Politecnico di Milano. Software enhancements were implemented to model air intake and separated/mixed-exhaust nozzles, enabling the evaluation of aircraft engine performance. Subsequently, the design and simulation of novel plant solutions were conducted to exploit the cooling potential of liquid hydrogen, resulting in a 4% improvement in thrust-specific energy consumption during the transition from conventional jet fuel. The findings suggest potential future developments, emphasizing the need for further exploration of the benefits of these systems while simultaneously facing challenges related to storage, combustion, and hydrogen production, which currently constrain their techno-economic feasibility. This research contributes to ongoing efforts for environmentally friendly aviation solutions, aligning with the Net Zero Emissions by 2050 Scenario.

Key-words: hydrogen, simulation, aircraft, turbofan, propulsion, air intake, nozzle

1. Introduction

Civil aviation provides an essential transportation network that connects the world and supports global economic growth. To maintain these benefits while meeting environmental goals, next-generation aircraft must have drastically reduced climate impacts. International passenger activity more than doubled in 2022 compared to the previous year, closing the gap with pre-Covid levels. The reopening of international travel in China provides an outlook for even higher growth from the beginning of 2023, with passenger and cargo activities returning to pre-pandemic levels [1]. In 2022 aviation accounted for 2% of global energy-related CO_2 emissions, having grown faster in recent decades than rail, road or shipping. As international travel demand recovers following the Covid-19 pandemic, aviation emissions in 2022 reached almost 800 Mt CO_2, about 80% of the pre-pandemic level. CO_2 emissions are expected to grow rapidly and to surpass their 2019 level around 2025. Many technical measures related to low-emission fuels, improvements in airframes and engines, operational optimisation and demand restraint solutions are needed to curb growth in emissions and try to reduce them this decade in order to get on track with the Net Zero Emissions by 2050 (NZE) Scenario [1].

Alternative aviation fuels include bio-jet fuels (fuels of the "kerosene type," produced from biomass), synthetic jet fuels (kerosene-type fuels produced from natural gas and coal), liquefied natural gas (LNG), liquefied hydrogen (LH_2) and electricity. Hydrogen has the highest heat of combustion and the highest specific heat of any of the candidate fuels. As versatile energy carrier that can be produced from a wide range of primary energy sources, H2 can additionally improve the reliability of the fuel supply for aviation [34] as it could remove the geopolitical tensions associated with the concentration of fossil fuel resources in a small geographical region. The process used to produce hydrogen is not discussed here: we mainly focus on the behavior of the aircraft engine by analyzing the main operational aspects related to switching from conventional jetfuel to hydrogen. Hydrogen-powered aircraft have the potential to fly existing routes with no carbon emissions and reduce or eliminate other emissions. Interest in these aircraft is currently high, but hydrogen aircraft present technical and economic challenges. Despite its high calorific value, hydrogen is known to be a fluid with low energy density on a volumetric basis. Aircraft designers must exercise ingenuity to find an aircraft configuration which will accommodate a fuel volume more than four times that which would be required for conventional jet fuel [20]. The density of LH_2 is two times greater than for compressed gaseous H_2 at 700 bar. Therefore, LH_2 is frequently considered the prime candidate for H_2 storage in aviation. Handling and storing hydrogen is challenging, particularly as a liquid. For H_2 fuel, the liquefication of gaseous H_2 requires compression and the removal of large amounts of heat. The liquefaction process consumes about 25% of the energy content in hydrogen [23]. In addition, because LH_2 is a cryogen, the space for the fuel must be amenable to providing an acceptable surface-to-volume ratio to minimize heat leak and weight of tank structure and insulation. Storing hydrogen as a liquid adds complexity to the fuel system, but it also offers possible synergies because a cryogenic fuel, especially when characterized by high specific heat, can be used as a heat sink.

Aim and structure of the report

This thesis work stems from the participation of the Department of Energy of the Politecnico di Milano in a European project called EFACA (Environmentally Friendly Aviation for All Classes of Aircraft). The EFACA project focuses on six main objectives:

1. Design, develop, and test a novel hybrid propulsion system that combines the power of a gas turbine engine with an electric motor.
2. Conduct comparative tests on two hydrogen fuel cells, one with conventional liquid cooling and the other with phase cooling, demonstrating the superior performance of the latter.
3. Test a complete liquid hydrogen power system, from the cryogenic tank to fuel vaporization and combustion.
4. Design a regional 80-seat turboprop aircraft with a range of 1000 km using hybrid turboelectric propulsion.
5. Design a 150-seat jetliner with a range of 2000 km that utilizes liquid hydrogen fuel.

This work is part of objective n°3 and aims to perform a comprehensive numerical analysis of the overall system to evaluate feasibility and performance via a proprietary owned computer code already developed and in use by Politecnico di Milano.
In section 2, we provide an overview of relevant studies conducted by researchers, organizations, and companies in the aeronautical sector. Section 3 presents the calculation methodology and the mathematical model used to describe the new components.
Although this initial software improvement work may not be groundbreaking, it is an essential component in this context. Nonetheless, it contributes to a deeper understanding of both the overall system and the logic behind the simulation code used.
Section 4 describes the reference engine chosen as the basis for the validation process and hydrogen configurations. Changes to the cycle architecture to make the most of the potential of liquid hydrogen are then discussed and detailed. Section 5 is devoted to the presentation of the results obtained, explaining their effects and implications. The final conclusions drawn from the research work, together with the proposed ideas for possible future developments, are presented in Section 6.

2. Literature review

Conducting a literature review for a comprehensive analysis of optimal aircraft engine design solutions involves first presenting the main types of available propulsion systems. This decision should consider both design constraints and environmental factors. Once the foundational architecture is selected, potential enhancements will be evaluated to assess their impact on the themes addressed in the subsequent study.
Fuel cells appear to be the dominant choice for small, short-range aircraft, while hydrogen combustion dominates for large, long-range aircraft [13]. Fuel cells are preferred for smaller aircraft because, unlike turbomachinery, their efficiency is relatively constant across a wide range of sizes. This is because the electrical current a fuel cell can produce is approximately proportional to the active area available for the reactions to take place; doubling

the active area roughly doubles the current. Furthermore, this technology is not affected by significant economies of scale. Fuel cells' ability to scale down and maintain their efficiency and specific cost can enable higher efficiency propulsion systems for these aircraft than is possible with hydrogen combustion. As the propulsion system power requirements increase, combustion eventually displaces fuel cells. This is because turbofans have higher specific power and fewer thermal management challenges than fuel cells; a fuel cell propulsion system for a 737-sized aircraft would be three times heavier than a similarly-sized turbofan system [13].
Most of today's commercial aircraft are powered by turbofan engines, where a large fan is driven by a gas turbine engine. The turbofan takes in surrounding air by the engine inlet, some of which passes through the fan to the compressor and then to the burner where it is mixed with fuel, and combustion occurs. Then, hot exhaust gas passes through the turbines and moves towards the nozzle, producing thrust. Most of the air pushed by the fan bypasses the engine core through a duct to create additional thrust. Due to the extra thrust by the fan-bypass air, it produces higher thrust for nearly the same amount of fuel used by the core and becomes more fuel-efficient.
The concept of a hydrogen-powered gas turbine remains the same as kerosene-powered engines, and thus engineers can leverage the previous experience. Because of the high specific power and historical engineering experience with turbomachinery, hydrogen combustion is the proposed solution for many hydrogen aircraft—particularly those from airframers and aircraft engine manufacturers. The four largest commercial aircraft engine manufacturers (GE Aerospace, Rolls-Royce, Pratt & Whitney, and Safran) have all published plans to build and test hydrogen combustion aircraft engines. CFM (a joint venture between GE Aerospace and Safran) is modifying a GE Passport turbofan to run on hydrogen. Airbus plans to fly the modified engine on an A380 demonstrator with liquid hydrogen tanks by around 2025 [2] and announced its ZEROe project in 2020 to develop clean sheet commercial hydrogen aircraft [3], shown in Fig. 1.

Figure 1: Airbus' ZEROe hydrogen-powered turbofan concept (Airbus image)

Pratt & Whitney announced its HySIITE project, funded by ARPA-E, to develop an LH2 combustion engine with steam injection to reduce NOx emissions [4].
Koç et al. [35], investigated the performance of a 50 MW simple and recuperative gas turbine fueled by natural gas and hydrogen and reported the differences in thermal and exergy efficiencies.
To provide a reasonable estimate of the potential which might be realized with LH2 in a turbofan engine, an engine design task was included in a study performed by Lockheed-California Company for NASA-Langley Research Center in 1976-1978 [19]. Five candidate concepts for obtaining improved performance were suggested and evaluated in this study:

- Compressor air precooling: precooling the compressor inlet air reduces the requirement for compressor work and the benefit is a reduction in size and weight of the gas generator. Roughly a 1.86% improvement in SFC was achieved. However, detailed heat exchanger design analysis conducted later in the study indicated there was a severe air-side freezing problem. Recirculation of warm fuel was investigated as a potential solution but it did not appear to be practical;
- Compressor air intercooling: the benefits are derived from the same reasons mentioned above, and the advantages also stem from the same reasons mentioned above, but placing the exchanger in a place where the air is warmer reduces the risk of the air freezing. This solution results in a 1% improvement in SFC relative to the baseline cycle;
- Cooling of turbine cooling-air: This concept consisted of using the hydrogen fuel to cool the air which is then used to cool the high pressure turbine. The thought was that using cold air to cool the turbine would reduce the quantity required to be extracted from the compressor. The maximum benefit to the cycle was approximately 0.53% improvement in SFC.
- Regenerative fuel heating: the scheme suggested for evaluation is essentially a regenerative gas turbine cycle except that the energy is added to the fuel rather than the air. In addition to the cost, weight,

and complexity issues, a difficult temperature control must be considered: achieving precise temperature control of the preheated fuel can be challenging as the load changes. Variations in fuel temperature can impact combustion efficiency and engine performance. In light of these warnings, the actual reduction in SFC is around 4%.

- Expander cycle: This concept involved providing aircraft accessory power by using a hydrogen expansion turbine. Originally it was hoped that the expander cycle could provide some of the fan or compressor horsepower requirements. However, preliminary calculations showed that the fuel would have to be pumped to very high pressures to provide significant amounts of power relative to the requirements of the fan and compressor. For example, 2000 psi is required to produce 580 hp, which is only 5% of the compressor horsepower. It is believed that the increase in engine complexity required to use the hydrogen expansion turbine to provide only a small amount of the compression horsepower requirements is not warranted.

In 2000, the European Commission funded the Cryoplane study [52] for the system analysis of hydrogen-fuelled aircraft. Different aircraft configurations were studied using a minimal change approach where the wing platform and engine design were unaltered when converting from kerosene to hydrogen. The study concluded that, due to the excessive tank volume required for LH_2, energy consumption would increase with 9-14% depending on the aircraft type.

Although previous research has explored the thermodynamic potential of hydrogen as a turbofan engine fuel, this study takes a comprehensive approach. It evaluates the benefits of using liquid hydrogen as a heat sink in order to improve engine performance. This analysis leverages in-house software equipped with advanced cooled-turbine calculation routines [22]. The goal is to provide an in-depth reference and basis for future advancements in this field.

3. Methodology

3.1. Gas Turbine Simulation Program

The realm of aeronautics relies heavily on the thermodynamic modeling of gas turbines. Various computer models are available to predict gas turbine performance and simulate their behavior. These engine models serve as mathematical representations of the physical behavior of the engine. They find applications in both the engine design phase and during its operational life.

The choice of model depends on several factors, including the engine's life cycle stage, the required level of accuracy, and the specific area of interest. These models aren't limited to thermodynamics; they can extend to areas such as vibrational analysis, which entails additional parameters for precise modeling, primarily catering to engine designers [17].

These models can be classified based on the spatial dimensions they consider, ranging from 0-D to 3-D. The dimensionality of the model affects the computational requirements:

- 0-D Models: These models compute flow properties at discrete points within the engine, typically correlating with the inlet and outlet of various components like the compressor. At these points, only average properties are calculated.
- 1-D Models: In 1-D models, average flow properties are continuously known throughout the engine. Instead of discrete points, one dimension of the engine, such as length, is continuously computed.
- 2-D Models: These models assume axi-symmetry in the flow. They involve modeling the physics behind the gas turbine processes.
- 3-D Models: 3-D models do not rely on simplifications and use the full equations of motion to represent the flow inside the turbine. These models are computationally intensive due to their complexity.

Each model type serves specific purposes in understanding gas turbine behavior, catering to different stages of the engine's life cycle and design processes. In this report, we will primarily explore thermodynamic modeling for performance calculations.

3.1.1 The GS code: background informations and working principles

In this study, performance predictions were conducted using the in-house developed software "Gas Steam" (GS). This tool has been developed since early 90's at the Energy Department of Politecnico di Milano over several years of dedicated work on energy systems. The programming environment is Fortran 90, programming language particularly suitable for numerical calculation, widely tested for the solution of engineering tasks. It provides accurate results in a variety of complex power and chemical plant configurations, including gas turbine cycles, combined cycles, coal based power plants and hybrid cycles [51].

The software, described in more detail in the work by Chiesa and Macchi [22], possesses a remarkable ability to

replicate intricate plant configurations by assembling fundamental modules representing the physical components (e.g. compressors, combustor, heat exchangers) of the system considered, in order to provide an interconnected network of elements, which constitutes the system under consideration. Upon adding a component its properties can be altered in the input file interface. Here the design parameters can be changed, which dictate the design point of the component. For a compressor this would for example be the design pressure ratio and efficiency amongst others. During a calculation run, mass and energy balances are computed sequentially for each component, applying appropriate operating characteristics and constraints. The iterative process continues until convergence is achieved, guaranteeing stable values for variables and satisfying all constraints. Given the iterative computational nature of GS, it necessitates an initial approximation as input. This initial solution consists of pressure, mass flow, temperature, and composition data for all the thermodynamic points within the system.
An essential aspect to be considered for the scope of this thesis work is the versatility of GS, as it allows for the incorporation of subroutines to simulate new components. This is noteworthy because the code, initially developed for analyzing stationary power plants, was able to be adapted through the addition of routines for nozzles and air intakes, elements needed in jet engines for aircraft applications.
All components, except for the turbine, are calculated using a 0-D approach, where the fluid conditions are known only at the inlet and outlet, without regard to the internal mechanisms that produce its change of state. The code incorporates a crucial one-dimensional design feature for gas turbine stages. This functionality enables the precise determination of essential parameters, including aerodynamic, thermodynamic, and geometric characteristics of each blade row. Notably, it allows for a detailed assessment of cooling flows and the evolution of cooled expansion, factors vital in understanding the performance of advanced gas turbines. The cooling model within the software accounts for complex aspects such as film cooling, thermal coatings, and multi-passage internal channels with enhanced heat-transfer surfaces. These effects are evaluated using calibrated parameters, ensuring the accurate representation of advanced gas turbine performance, as outlined in Ref. [22]. If a code capable of simulating the behavior of a cooled gas turbine is crucial for stationary application, it becomes even more vital when simulating the performance of a modern turbofan engine. Such engines are characterized by turbine inlet temperatures typically exceeding those of stationary cases, aiming to ensure higher performance alongside more frequent component replacements and consequently, higher maintenance costs. In particular, this holds true for rotors, which experience substantial thermal stresses due to centrifugal forces. Viscous creep is a primary factor contributing to the mechanical stresses induced by high temperatures. Under its influence, even slight increases in the material's operating temperature can result in significant reductions in the component's service life.

3.1.2 Design and off-design simulations

To better understand the capabilities and limitations of GS in the context of the presented work, it is crucial to clarify the fundamental difference between design simulation and off-design simulation.
Design point performance serves as the cornerstone of the engine concept design process. During this phase, the engine's configuration, cycle parameters, component performance levels, and sizes are chosen to meet the required specifications.
For the purposes of this work, achieving a design simulation that accurately represents the reference engine's operational parameters stands as a crucial step. This is by far the first step to validate the proper functioning of the added components and for proceeding with further in-depth analyses, optimization, and assessment of potential constructive improvements (Section 4.5).
On the other hand, off-design point performance characterizes the steady-state performance variations of a fixed engine design when operational conditions are altered. This involves finding a point on the map of each component which satisfy the compatibility conditions, which can be identified in mass flow, work, and rotational speed balances across various engine elements.
For a twin-spool turbofan engine, this harmonization process has specific implications. It mandates that the rotational speeds of the fan, booster, and LPT must match, given their connection to the Low Pressure LP shaft. Similarly, the HPC and HPT must share the same rotational speed, connected to the HP shaft. Furthermore, the power generated by the LPT must be balanced with the power required by the fan and booster, while accounting for any mechanical losses. The same applies to the HPC and HPT on the HP shaft. The mass flow through the core engine must be evenly distributed across all components after considering any adjustments due to tertiary airflows. Consequently, even though the components on both shafts are mechanically uncoupled, they remain aerodynamically interconnected.
It's worth noting that design point performance must be established before delving into the analysis of any other operational conditions.
Off-design performance of components can be specified using component characteristics, or component maps. The GS software neither supports the loading of these maps nor has it been developed to perform the calculations necessary for the convergence of different constraints at the given point. However, in the realm of aviation

applications, more than ground power generation, conducting an off-design in-flight simulation is essential for a complete analysis. Hence, as detailed in Section 4.4, a simplified model of off-design in GS has been developed. In this context, the author used an external commercial software named GasTurb [5] to verify that the assumptions made in the simplified model were consistent. The cruising condition has been selected as the second point of analysis for two main reasons: the greater availability of data for comparison with the reference engine and the fact that the engine operates in this state for the majority of its operational time.

3.1.3 Verification of Thermodynamic Properties Calculations

The computational software utilized in our analysis relies on correlations from NASA Polynomials [40] to compute the thermodynamic properties of gases [43]. These correlations, however, are only valid within the temperature range of 300 to 5000 K, assuming ideal gas behavior. Given that our study extends to typical flight altitudes for passenger aircraft, the conditions often fall outside this temperature range. To ensure the accuracy of our calculations beyond these limitations, a comparative study was conducted using the REFPROP software [38]. The REFPROP's calculations regarding the thermodynamic properties of fluids are highly reliable in the field of engineering. This reliability is achieved by using equations of state calibrated for each fluid, taking into account real gas effects, which can become more significant at lower temperatures, as explained in more detail below. This analysis involves a temperature range from 200 to 2000 K, with pressure as the variable parameter, spanning from 0.1 bar to 10 bar. At the conclusion of the study, actual ambient temperature and pressure data, provided by the International Standard Atmosphere (ISA) for flight altitudes ranging from 0 to 12,500 meters, were employed to evaluate the actual errors within the context of aircraft flight condition.
For the purposes of this study, the specific heats of the three main constituents of air, N_2, O_2, and Ar, were initially calculated using NASA Polynomials correlations (with coefficients valid up to T = 300 K, even for the range 200 - 300 K). Subsequently, REFPROP was used to perform the same calculations. It's important to note that the accuracy of specific heat values serves as a good indicator that thermodynamic properties are calculated correctly. Specific heat is a fundamental property of materials, and its accuracy is crucial for calculating other thermodynamic properties such as enthalpy and entropy.
Other gases like water vapor and CO_2 were intentionally excluded from this analysis since their effects, given their very low concentrations, were considered negligible during engine operation. While these gases may not be the only species present when considering the engine as a whole, it's worth noting that temperatures lower than 300 K typically occur upstream of the LPC, where fuel has not yet mixed with air, and combustion (which introduces new species) has not yet occurred. Nevertheless, the most critical point is undoubtedly the starting point of the cycle, which is the undisturbed ambient air conditions under the considered flight conditions, potentially characterized by temperatures outside the range of 300 K - 5000 K.
The results presented in Fig. 2 show the relative deviation between the two calculated values expressed as a percentage, as formulated in (3.1).

$$\Delta C_{p,i\,\%} = \frac{C_{p,NASA} - C_{p,REFPROP}}{C_{p,REFPROP}} \cdot 100 \tag{3.1}$$

The deviations within the range of validity of NASA Polynomials are very small, remaining below 2% for all species at different pressures. In the most critical conditions, i.e., at $P = 10\,bar$ and $T = 200\,K$, deviations increase for all three species, reaching up to 3.5 - 6.2 percentage points.
As expected, the absence of coefficients suitable for low-temperature calculations and the assumption of ideal gas behavior impact the accuracy of the GS software calculations. Under low-pressure conditions, real gases behave very similarly to ideal gases. However, at higher pressures, intermolecular forces become more significant, causing real gas behavior to deviate from ideal gas behavior. Additionally, at lower temperatures, gas molecule kinetic energy is lower, making them less likely to overcome intermolecular forces that hold them together.
In this context, it's important to note the role of pressure in calculating thermodynamic properties in gas cycles: The assumption that air and air-fuel mixtures behave as ideal gases at typical operating pressures of a gas cycle is reasonable but not entirely accurate. As pressure increases, intermolecular forces become more significant, causing real gas behavior to deviate from ideal gas behavior. Gas turbine pressures typically range from 10 to 70 bar. At these pressures, the effects of real gas behavior are generally negligible, but it's essential to remember that they can become significant at higher pressure conditions.
Finally, in Fig. 3, deviations are presented concerning variations in flight altitude at temperature and pressure values according to the International Standard Atmosphere (ISA).
When considering the actual conditions under which the inflow exists, a significant reduction in deviations can be observed. In this case, the maximum values are less than 0.5%. This reduction is mainly attributed to the combination of decreasing temperature and pressure at higher altitudes, which mitigates the effects of real gases, rendering the ideal gas assumption more valid. In conclusion, due to the limited impact of a more accurate calculation of thermodynamic properties on the problem at hand, it was decided to proceed with the use of the original NASA Polynomials relations implemented in GS.

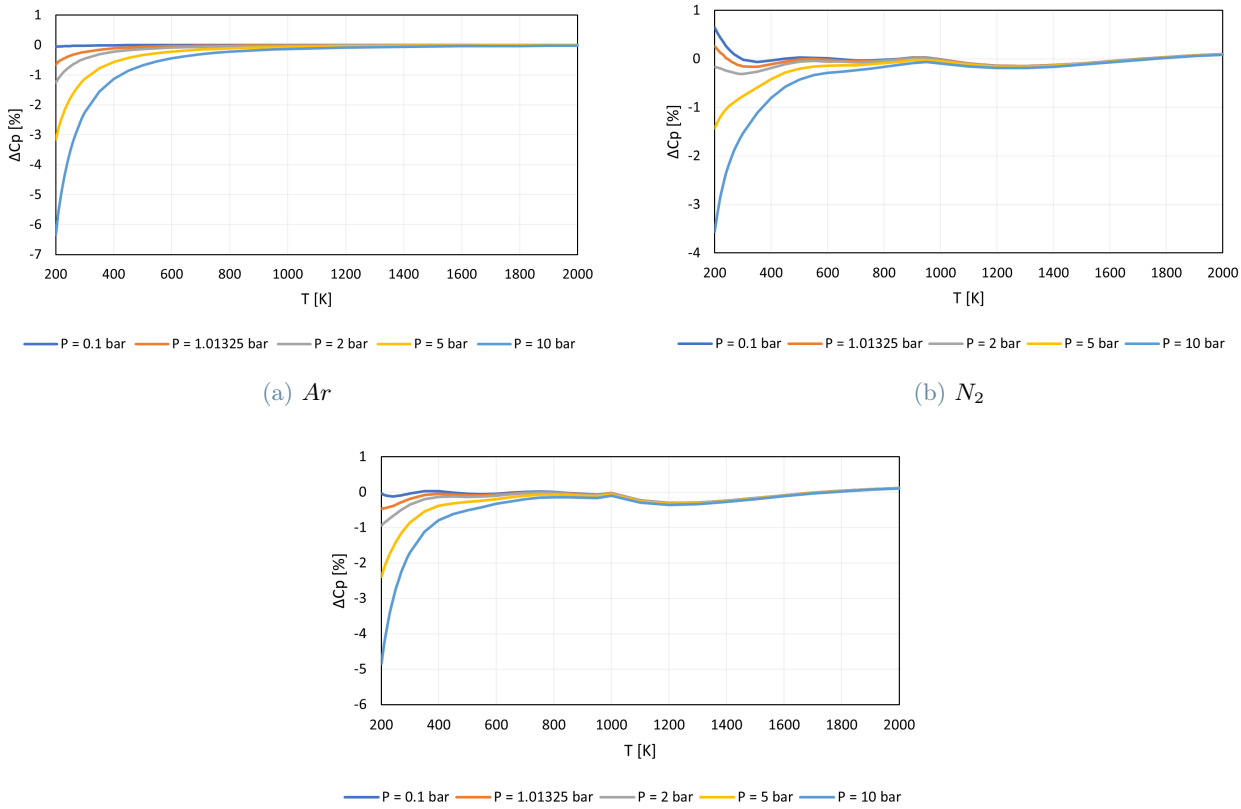

(a) Ar

(b) N_2

(c) O_2

Figure 2: Specific heat percentage deviations varying T and P for pure air constituents

3.2. Modelling of Air Intakes and Nozzles in GS Software

As previously mentioned, the GS software lacked computational codes for simulating dynamic intakes and nozzles. The following sections address the need for incorporating these components and outline the methods by which they were modeled.
Given the significant role that fluid velocity plays in the thermodynamic calculations of both components and its influence on the determination of propulsive thrust, along with all the associated parameters, and the fact that static variables underpin the definition of the isentropic efficiency of the nozzle, as will be discussed in detail later, it was decided to consistently monitor fluid velocities upstream and downstream of both modeled components. This approach also facilitated result validation by providing a wide range of parameters for comparison with existing turbofan application. In line with established literature, the assumptions regarding the Mach numbers at the turbine exit (nozzle inlet) and the fan inlet (intake exit), have helped the writer to actively control the passage areas and avoid mistakes.

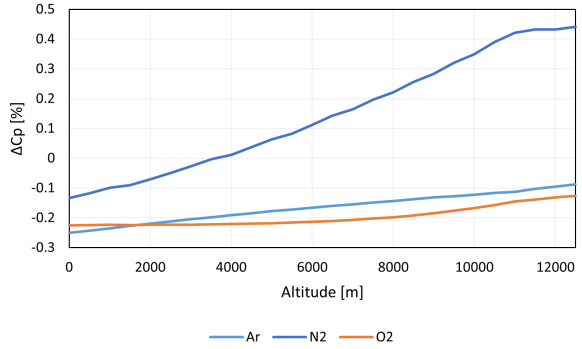

Figure 3: Specific heat percentage deviations varying altitude for pure air constituents

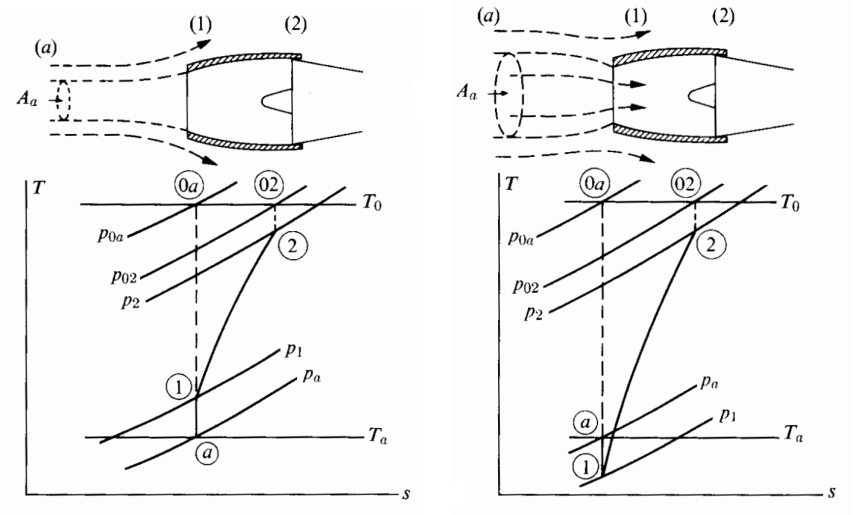

(a) *High speed or low mass flow* (b) *Low speed or high mass flow*

Figure 4: Typical streamline patterns for subsonic inlets [31]

The characterization of these two components is conducted within the domain of subsonic flows. This is due to the fact that the aircraft of interest are equipped with typical turbofans found in passenger airliners, operating in a subsonic regime at the intake and, at most, a transonic regime at the nozzle exit. Modeling these components under supersonic conditions is notably more complex, as it necessitates accounting for shockwave formation (highly irreversible phenomenon) to obtain an accurate estimation of stagnation pressure losses.
Both the processes are very close to adiabatic, since the heat transfer per unit mass of fluid is much smaller than the difference in enthalpy between inlet and exit. Along with the fact that there are no moving parts that can introduce or extract work from the system, it is a reasonable to assume, without introducing substantial errors, that the stagnation temperature remains constant between the inlet and the exit in both scenarios.

3.2.1 Air Intake

The effective operation of an aircraft engine depends significantly on the design and functionality of its air intake system. For jet engines, it's vital to maintain a low Mach number airflow in the range of 0.55 to 0.65 [50] as it enters the compressor or fan, with the higher end of this range reserved for transonic compressors or fans. These values are higher than for axial flow compressors due to the need to minimise fan frontal area for aerodynamic and economic reasons. Ensuring that the airflow leaves the inlet uniformly is of paramount importance, as deviations in the velocity profile at the compressor inlet can disrupt the aerodynamics and potentially lead to blade failure due to vibrations.
Qualitatively the flow in the inlet behaves as though it were in a "diffuser", which is a common element in fluid machinery. Minimizing intake length is favorable not only for weight considerations but also to control total pressure losses tied to the development of a growing boundary layer as the diffuser length increases. However, in-depth studies suggest that longer intakes with smaller pressure gradients are necessary to avoid separation risks, which could result in increased total pressure losses and flow non-uniformity. Preventing separation requires maintaining the pressure gradient $\frac{dp}{dx}$ below a certain experimentally determined threshold, leading to the adoption of a minimum cone angle for the diffuser.
The intake must operate under varying incident stream conditions, depending on the aircraft's flight speed and engine mass flow requirements. During level cruise, the streamlines may involve deceleration external to the inlet plane, while low-speed, high-thrust conditions, such as takeoff and climb, necessitate more mass flow and result in an external acceleration of the stream before the inlet. Fig. 4 shows the streamline patterns for two typical subsonic conditions and the corresponding thermodynamic path of an "average" fluid particle. These conditions involve isentropic state changes without the presence of friction due to wall interactions. However, this behaviour has implications on the stagnation pressure losses, resulting in a dependency on both the engine's aspirated volumetric flow rate and the flight Mach number. Higher volumetric flow rates yield higher average flow velocities within the duct, resulting in increased fluid dynamic losses. Meanwhile, at higher flight Mach numbers, the deviation from the optimal design incidence angle of the flow tube with the outer ring of the dynamic intake is minimized, given the same aspirated volumetric flow rate. The relationship between these variables is depicted in Fig. 5. In the graph, the stagnation pressure ratio π_d is a function of the corrected engine airflow and the flight Mach number. Corrected engine air flow is the mass flow rate of air entering the

engine, corrected to standard sea level conditions. This means that the air flow rate is adjusted to account for the effects of temperature, pressure, and humidity. Corrected air flow is the mass flow rate of air entering the engine, corrected to standard sea level conditions. This adjustment accounts for the effects of temperature, pressure, and humidity on air density. Corrected air flow is used to compare the performance of engines operating in different conditions. For example, an engine operating at high altitude will have a lower uncorrected air flow rate than an engine operating at sea level. However, the corrected air flow rate for both engines will be the same. In other words, the volumetric flow rate will always be the same at a given corrected air flow rate.

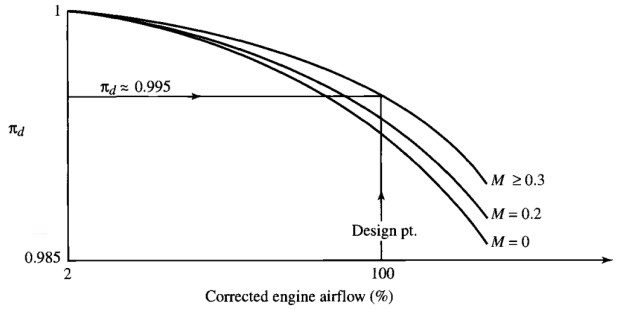

Figure 5: Typical subsonic inlet total pressure ratio [39]

The known fluid conditions are those infinitely upstream, specifically those of undisturbed ambient air at the considered flight altitude. The first step involves determining the specific heat ratio γ of air through a dedicated function within GS, with input parameters of ambient temperature and pressure. This process yields the speed of sound a that, coupled with Mach number at the entrance, provides the inlet flow speed. This allows for an evaluation of the total fluid conditions at the air intake inlet. It becomes evident that in the case of a fixed-point simulation, such as during takeoff (M = 0), the total thermodynamic variables at the air intake inlet plane remain the same as those of undisturbed ambient air. Subsequently, as per Fig. 5, the total pressure loss is considered and the total conditions are retained in the output file. For flight Mach numbers within the ranges of 0 to 0.2 and 0.2 to 0.3, a linear interpolation of the existing curves was employed to estimate the stagnation pressure ratio. Finally, the static conditions at the exit can be determined under the assumption of a Mach number at the fan inlet equal to 0.6. Particular attention should be directed towards this final step: an iterative cycle is necessary to determine the exit velocity at a known Mach number. This is due to the direct and indirect dependence of the speed of sound a on static temperature T, as described below:

$$a = \sqrt{\gamma \frac{R}{MM} T} \tag{3.2}$$

The indirect dependency is encapsulated within the specific heat ratio γ, given the choice to consider the variation of specific heats with temperature. For added clarity, the pseudocode for this iterative cycle is presented in Algorithm 1.
The iterative scheme presented will be used whenever the total variables and the Mach number are known, and we want to estimate the absolute velocity and static conditions of the flow. This is also the case when determining the velocities of the hot and cold flows as they exit the LP turbine and the fan, respectively.

Algorithm 1 While cycle to assess the static conditions and velocity of the flow entering the fan

$\gamma = f(T_T)$ as a first guess
$v_{in,fan} = M_{in,fan} \sqrt{\gamma \frac{R}{MM} T_T}$
$\varepsilon = 10^{-6}$
while $h + \frac{v_{in,fan}^2}{2} - h_T > \varepsilon$ **do**
    $h = h_T - \frac{v_{in,fan}^2}{2}$
    $s = s_T$ by definition
    $T = f(h, s)$
    $P = f(h, s)$
    $\gamma = f(T)$
    $v_{in,fan} = M_{in,fan} \sqrt{\gamma \frac{R}{MM} T}$
end while

3.2.2 Nozzle

A crucial component of jet engines, the propulsive nozzle, transforms thermal energy into kinetic energy, generating thrust by expelling high-speed propulsive fluid. This transformation occurs through an expansion process, controlled by pressure. Its role remains qualitatively consistent but varies quantitatively depending on whether the engine is a ramjet, turbojet, turbofan, turboprop, or turboshaft. In fact, in a ramjet, the entire enthalpy drop available downstream of the combustion chamber is exploited in the nozzle, while in turbojets, the work extracted by the turbine necessary to drive the compressor lowers the available enthalpy drop available at the nozzle. The magnitude of the work extracted in the turbine is more substantial for turbofans, where the turbine must power both the compressor and the fan. Specifically, as we have seen, in turboprops, it represents a significant portion of the available enthalpy drop. In the case of turboshafts, the entire available enthalpy drop is employed in the turbine, so the nozzle primarily acts as an exhaust duct.
In order to accurately predict the thermodynamic performance of the propulsive nozzle, the two main sources of losses have to be described as follows:

- **Fluid Dynamic Losses within the duct:** These losses arise from unavoidable friction phenomena and possible boundary layer separation. Notably, nozzle separation issues are comparatively minor and easier to prevent than diffusers because the flow operates with a favorable pressure gradient. Coefficients are commonly employed to estimate real flow conditions at the outlet concerning ideal (or equivalently, isentropic) conditions. The accurate estimation of these losses heavily depends on the geometric variables of the duct, such as the area ratios, cone opening angle, surface roughness, and so on. However, it's important to note that this thesis does not focus on the detailed geometric characterization of the engine components. Moreover, from an overall system perspective, an efficiency variation of 1-2 percentage points does not significantly impact the engine's performance as a whole. Therefore, adopting an isoentropic efficiency η_n as defined in Eq. (3.3) has been considered a suitable compromise between modeling simplicity and result reliability.

$$\eta_n = \frac{h_{T,in} - h_{out}}{h_{T,in} - h_{out,is}} \tag{3.3}$$

- **Losses Downstream of the Exit Section:** As long as the expansion ratio remains below the critical ratio (the ratio at which a sonic flow with M = 1 establishes in the nozzle exit section), the flow in the duct is entirely subsonic. It progressively accelerates, expanding until ambient pressure is reached. When the external pressure equals the critical pressure, perturbations from the downstream environment cannot propagate back along the duct because the absolute velocity of incoming perturbations (propagating at the speed of sound as well) is zero at the exit section. Consequently, for any external pressure below the critical pressure, the flow remains blocked in a sonic flow condition in the throat (choked nozzle). This sonic blockage dictates that the jet pressure at the nozzle exit must exceed ambient pressure. As the flow exits the nozzle and is no longer confined by duct walls, it further adapts to external conditions through additional expansion. In these cases, the nozzle is termed "under-expanded." This supersonic post-expansion leads to jet widening, effectively making the fluid vein divergent. However, post-expansion is associated with significant losses due to interactions between the jet and the external environment and between expansion and compression waves within the jet, resulting in substantial performance reductions compared to the adapted case. For the evaluation of net thrust propulsion, it was not necessary to introduce any additional parameters to assess this loss. As clarified in Appendix A.1, the momentum balance within the system allows bypassing the modeling of losses downstream of the nozzle exit section.

The presence of two distinct flows offers the possibility of various configurations, with the primary distinction being between separate exhaust turbofans and mixed-stream turbofans.
Mixed-stream turbofan engines, where the core and bypass streams are mixed before expansion, are now increasingly considered for use in civil aircraft in addition to their extensive military application. Compared to separate exhaust turbofans, the main thermodynamic advantage of the mixed-stream concept is an improvement of about 2–3% in specific thrust and thrust-specific fuel consumption [29][44]. Although these improvements may seem marginal, they hold significant value over the entire service life of the aircraft. The theoretical and experimental details of the mixing process and the basis and magnitude of the resulting performance gains in comparison to separate exhaust turbofans can be found in Ref. [29][44].

How mixing increases thrust Let's consider a simplified graphical example to illustrate how mixing enhances thrust. Suppose we have a bypass ratio of unity ($\dot{m}_{hot} = \dot{m}_{cold} = \dot{m}$) and equal pressures in both the core and bypass ducts before mixing. The core stream has a significantly higher temperature compared to the bypass stream, resulting in differing enthalpy values.
If both the hot and cold streams are expanded to the prevailing ambient pressure, the changes in enthalpy correspond to the changes in kinetic energy. In this scenario, the total thrust T_{unmix} can be calculated as

follows:

$$T_{unmix} = T_{hot} + T_{cold} = \dot{m}\sqrt{2}\left(\sqrt{\Delta h_{hot}} + \sqrt{\Delta h_{cold}}\right) \tag{3.4}$$

If the hot and cold streams are mixed completely

$$h_{mix} = \frac{h_{hot} + h_{cold}}{2} \tag{3.5}$$

and the total thrust T_{mix} is:

$$T_{mix} = 2\dot{m}\sqrt{2\Delta h_{mix}} \tag{3.6}$$

Fig. 6 shows the $T - s$ diagram for separate hot and cold streams as well as a mixed stream for the current situation. It may be seen that the mixed specific enthalpy is the average of the hot and cold stream values, but because the isobars diverge as enthalpy increases, the mixed stream kinetic energy Δh_{mix} is closer to that of the hot stream than to the cold stream and twice its value is always greater than the sum of hot and cold. Therefore:

$$T_{mix} > T_{unmix} \tag{3.7}$$

This reasoning can easily be applied to more practical cases where the hot and cold flows are not equal. This overall performance enhancement can be viewed from two perspectives. Firstly, an engine with mixed flows can provide higher propulsive efficiency compared to separated flow engines at the same thermal efficiency. Alternatively, when studied at a constant propulsive efficiency, it results in lower fuel consumption and, consequently, higher thermodynamic efficiency.

A more in-depth exploration is required to fully understand how the operational parameters change between these two different design solutions. A study with a fixed bypass ratio and a variable β_{fan} can aid in comprehending the differences. The mixing of flows introduces an additional design constraint, as static pressures of the core and bypass streams at the mixer inlet must be equal at all flight points before mixing, constraining the variation of β_{fan}. In the case of separate flows, this ratio can be chosen freely, within other constraints. A parametric study on the fan compression ratio for the separate flow solution can demonstrate that an optimal β_{fan} exists [50], as it affects performance. At low fan pressure ratios, excessive core jet velocity wastes energy, as does the bypass jet velocity at high fan pressure ratios. There's also energy wastage in the inefficiency of energy transfer from the core to the bypass stream, as the LP turbine and fan bypass efficiencies are less than 100%. The optimal ratio of bypass jet velocity to that of the core is simply the energy transfer efficiency, which is the product of the LP turbine and fan bypass efficiencies. The optimum core jet velocity is therefore consistently higher, by a factor of around 1.2, as the optimum would be equal velocities if the energy transfer efficiency were 100% [50].

At this point, an honest comparison between the optimal separate flow and mixed-stream solutions is needed. Consequently, the performance differences between these two engine architectures are not substantial, but the components on the low-pressure spool vary significantly. The optimized fan pressure ratio is significantly lower for a mixed engine [42][36]. The magnitude of this reduction increases as bypass ratio is reduced. As a result, the pressure ratio of the mixed flow turbofan LPT is much lower. This offers an opportunity to compensate for the added weight of the mixer with a reduced number of LP turbine stages and a lower low-pressure spool speed. It's also worth considering that in the case of separate flow turbofans, cost and weight savings can be achieved by siting the nozzle of the secondary flow immediately downstream of the fan. On the other hand, the

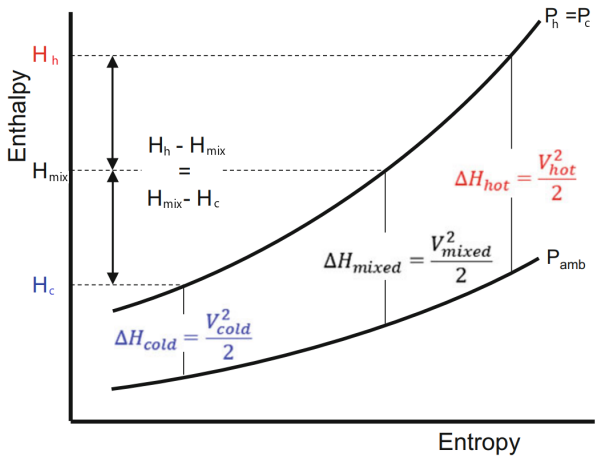

Figure 6: T-s diagram for unmixed and mixed nozzles

associated flow configuration involves the creation of a mixing chamber downstream of the low-pressure turbine, along with the necessary presence of a duct to guide the cold flow. The addition of components not present in the other configuration should be carefully evaluated in the design process.

Modeling and calculation of the mixing chamber A simplified model has been employed to account for losses in the mixing process and a non-uniform temperature distribution at the end of the mixing chamber [18]. As seen in Eq. (3.11), a mixing efficiency, denoted as η_{mix}, has been directly integrated into the momentum balance equation. Lobed annular mixers are preferable in this context. With higher bypass ratios, it becomes increasingly difficult to achieve a uniform temperature distribution, so mixing efficiency drops. This, coupled with the decreasing outperformance as the bypass ratio increases, leads to the conclusion that mixed flow turbofans offer better thermal efficiency and SFC only for modest bypass ratios.
It is worth noting that the inefficiencies have deliberately been allocated only to the velocity components in Eq. (3.11). This choice is supported by the nature of the fluid dynamic losses that occur during mixing, primarily attributed to the transformation of kinetic energy into thermal energy due to turbulence, as well as friction with both the walls and between the interacting fluid molecules. Indeed, these losses are directly proportional to the inlet velocities of the two streams.
It's important to emphasize that this approach is considered preliminary, and for more detailed calculations, a CFD simulation performed on a geometric model that accurately represents reality would be the more suitable choice. It's important to clarify that all the considerations presented earlier are valid for relatively high mixing efficiencies ($\eta_{mix} > 85 - 90\%$). Excessive deviations from ideality may not yield any thermodynamic benefits and, in the most extreme cases, could lead to a degradation in engine performance. However, the geometric simplicity of the problem at hand, the use of a not very high BPR (about 5) as will be seen later, together with the assumption of well-designed components, enables operation with such high efficiencies. For this reason, a constant $\eta_{mix} = 95\%$ was adopted in this study.
As the flow rates and thermodynamic properties of the two inlet streams to the combustion chamber are known from the calculations of the fan and LP turbine, the inlet areas A_1 and A_2 can be calculated as follows:

$$\rho_{in,1} = \frac{p_1 MM_1}{RT_1} \quad \rho_{in,2} = \frac{p_2 MM_2}{RT_2} \tag{3.8}$$

$$A_1 = \frac{\dot{m}_1}{\rho_{in,1} v_1} \quad A_2 = \frac{\dot{m}_2}{\rho_{in,2} v_2} \tag{3.9}$$

To determine the downstream flow conditions (P_out, $T_{T,out}$, v_{out}) of the mixing chamber, we need to solve the three balance equations: mass balance (3.10), momentum balance (3.11), and energy balance (3.12):

$$\dot{m}_1 + \dot{m}_2 = \rho_{out} v_{out} A_{out} \tag{3.10}$$

$$(\dot{m}_1 v_1 + \dot{m}_2 v_2)\eta_{mix} + p_1 A_1 + p_2 A_2 = \dot{m}_{out} v_{out} + p_{out} A_{out} \tag{3.11}$$

$$\dot{m}_1 h_{T,1} + \dot{m}_2 h_{T,2} = (\dot{m}_1 + \dot{m}_2) h_{T,out} \tag{3.12}$$

The ideal gas equation of state (3.13), which relates pressure P, static temperature T, and density rho, should be added to the system. In addition, under the assumption of ideal gases, static enthalpy and total enthalpy are solely functions of static temperature and total temperature, respectively, and vice versa. Thus, static temperature can be calculated from the stagnation temperature, related to the total enthalpy obtained from (3.12), using (3.14).

$$\rho_{out} = \frac{p_{out} MM_{out}}{RT_{out}} \tag{3.13}$$

$$h_{out} = h_{T,out} - \frac{v_{out}^2}{2} \tag{3.14}$$

where MM_{out} is calculated through the conservation of individual species in the two streams, assuming no chemical reactions occur.
At this point, an additional equation is needed to equalize the number of unknowns and equations, which is imposed by the design choice of the component under consideration.
In this context, two different approaches for modeling the mixing chamber have been described:

1. Constant exit section equal to the sum of the inlet areas of the two flows:

$$A_{out} = A_1 + A_2 \tag{3.15}$$

2. Isobaric mixer, which implies a variable-geometry exit section that depends on the operating conditions:

$$p_{out} = p_1 = P_2 \tag{3.16}$$

In both cases, one of the problem's unknowns is calculated explicitly. The energy balance also explicitly provides the total enthalpy at the exit. The resulting system consists of 4 equations implicit in 4 unknowns. The Newton-Raphson iterative method, based on finite difference derivative calculations, has been employed to solve the problem.
In case 2, computational effort can be reduced if, with the assistance of Fig. 7, one observes how the pressure contributions mentioned in (3.11) account for the conical wall (a cone-shaped wall is necessarily present when the exit area differs from case 1). Specifically, only the axial component of the resultant force R acting on the entire truncated cone section is relevant to the problem at hand. In this scenario, the flow velocity can be directly calculated, simplifying the problem to the resolution of a series of explicit equations in the order (3.11), (3.14), (3.13), (3.10).

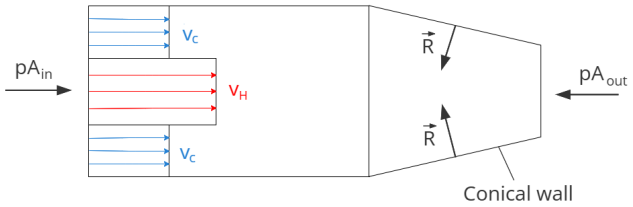

Figure 7: Forces acting on the mixing chamber

4. Case study

To successfully validate the mathematical model used, the ideal scenario involves referencing experimental data of a representative engine provided by the manufacturer or airline. These measurements are typically conducted by the manufacturer on a test bench and by the airline through on-wing measurements, where the engine is mounted on the wing and enclosed in the nacelle. Such data furnishes highly reliable information about various thermodynamic points within the cycle, facilitating a more straightforward and immediate validation of the model.
Unfortunately, this proprietary data, along with the actual component maps, is not publicly available. However, informations from publicly accessible sources, such as:

- engine reviews containing Full Authority Digital Engine Control (FADEC) data, line basic maintenance documents and promotional material published by the manufacturer [15] [14];
- type certificate data sheets issued by the U.S. Department of Transportation Federal Aviation Administration (FAA) [25] and the European Union Aviation Safety Agency (EASA) [26];
- airline employee training manuals [27];
- a comprehensive review of relevant literature [31] [17] [50] [39] [49] [36]

have offered a comprehensive overview of the analyzed reference engine (details in Chapter 2.4) and the thermodynamic conditions at various points in the cycle.
For this particular study, the take-off scenario at International Standard Atmosphere (ISA) sea level conditions has been selected as the design point for the model. This choice is attributed to the fact that it represents a point with the most known parameters, making it a suitable reference point for the analysis. On the other hand, the cruise case will be considered as off-design operation.

4.1. Reference engine: General Electric CF6-80C2

For this study, GE CF6-80C2 was adopted as the reference engine for model validation. The General Electric (GE) CF6-80C2 jet engine is a dual-rotor, turbofan with a high bypass ratio, variable stator geometry and unmixed exhaust. It is shown in Fig. 8a.
The dual-rotor engine consists of both a LP shaft and a HP shaft. This configuration is necessitated by the high compressor pressure ratio and the limitations on fan speed. Achieving the required pressure levels demands a high rotation speed for the HPC. Simultaneously, the fan speed is constrained by aerodynamic, structural, and noise considerations, necessitating a lower rotation speed. Optimum design fan speed would be too slow for the HPC to compress enough air. Therefore the fan, the booster and the LPT rotate with a low speed on the LP shaft. The HP shaft consists of the HPC and the HPT.

The LPT in modern turbofans is characterized by a notably high number of stages. This design feature can be attributed to specific factors:

- **High Bypass Ratio (BPR):** In engines with a high bypass ratio, a substantial portion of the total airflow is directed through the fan rather than the turbine. The higher the difference between these mass flow rates, the more power is demanded from the fan compared to the power produced by the LPT.
- **Work is Proportional to Rotational Speed:** The work generated by the turbine is directly proportional to its rotational speed. However, due to the constraints aforementioned, the LPT rotational speed is limited. As a result, each turbine stage must manage a reduced enthalpy drop while maintaining its efficiency.

As a consequence, a high number of stages is required to handle the substantial overall enthalpy drop efficiently. The use of a geared turbofan can alleviate the mentioned issues related to the high number of stages in the LPT. A geared turbofan incorporates a reduction gearbox between the fan and the low-pressure spool. This allows the fan to rotate at a different speed compared to the rest of the engine components. The drawback is that it increases weight and adds complexity, both for maintenance and in the design phase.
As detailed in Fig. 8b, the engine configuration consists of a single-stage fan, a 4-stage booster, both driven by a 5-stage LPT. Additionally, a 14-stage HPC is balanced by a two-stage HPT. The initial five stator stages of the HPC are equipped with variable geometry kinematics. This feature allows for the reduction of flow areas while maintaining high air velocity at the stator outlet as the airflow diminishes under part-load conditions. This design approach prevents excessive flow incidence on the subsequent rotor stages, mitigating the risk of profile stall and the associated pumping effect. The annular combustor, where the air-fuel mixture is burned, is in between the HPC and the HPT.
As the HPT is one of the critical and most challenging components to design within the entire engine, the most relevant features, the materials used, and details regarding cooling flows are presented in Fig. 9.
This engine is classified as a high-bypass-ratio (BPR) turbofan because approximately 80% of the incoming airflow bypasses the core engine and is expelled through the fan duct, generating fan thrust. The fan provides about 80% of the engine thrust.
It is designed for subsonic commercial airline service. Introduced in October 1985, the CF6-80C2 is certified on 11 widebody aircrafts, including the Boeing 747 and 767, the McDonnell Douglas MD-11 and the Airbus A310. The choice of this particular propulsion system as a reference engine is based on the prior experience and knowledge of the research group at Politecnico di Milano regarding the GE LM6000 stationary gas turbine, which is derived from the selected aircraft turbofan. This ensured greater reliability in interpreting the obtained results and the ability to make reasonable assumptions about operational parameters when needed.
The primary focus of this study centers on the CF6-80C2B1F jet engine. The CF6-80C2 family comprises a total of 13 main variants [11], each having its own ratings and performance. These variants employ a two- or three-character suffix to denote the engine's intended application. Specifically, the 'B' designation signifies its use on Boeing aircraft, while "1" gives information about the specific aircraft model (in this case 747-400). The use of the third character 'F' signifying the presence of Full Authority Digital Engine Controls (FADEC). From this point onwards when referenced to a CF6-80C2 a CF6-80C2B1F is meant.
The main dimensions and technical specifications of CF6-80C2B1F are presented in Table 1, where cruise conditions correspond to a flight Mach number $M = 0.8$ at an altitude $z = 35000\,ft$ (which is equivalent to about $10500\,m$).

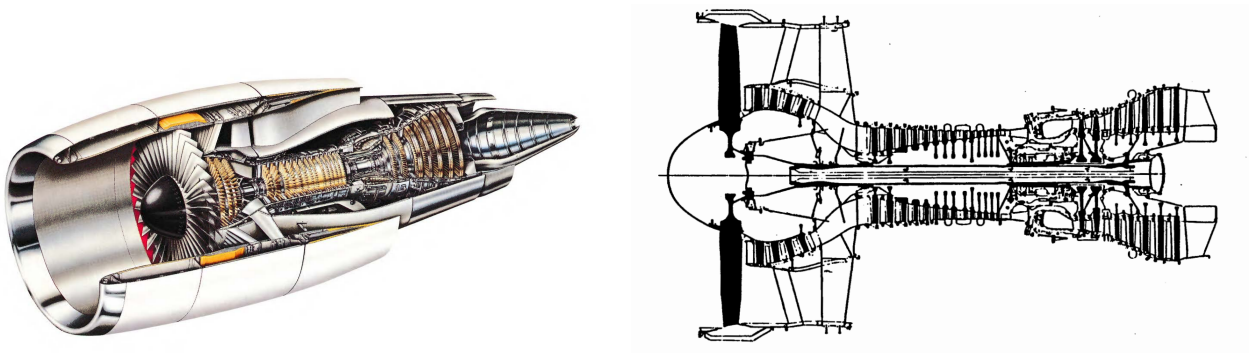

(a) *Configuration with nacelle included* (b) *Engine cross section*

Figure 8: GE CF6-80C2 turbofan

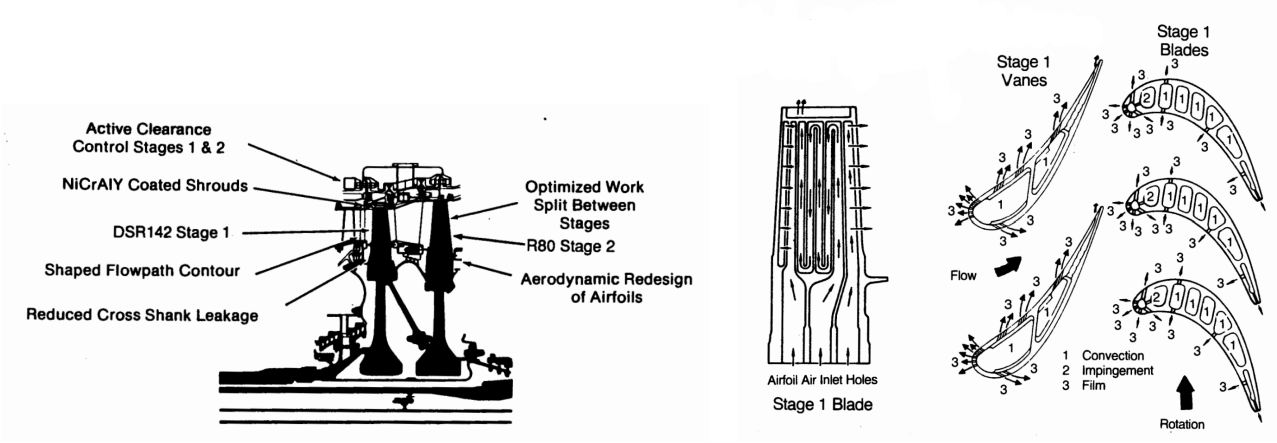

(a) *Main features and materials* (b) *Turbine blade and vane cooling techniques*

Figure 9: HPT deatails

Table 1: CF6-80C2B1F specifications

Length [cm]	427	Weight [kg]	4465
Fan diameter [cm]	236	# of fan blades [-]	38
Takeoff airflow rate [kg/s]	795	Cruise thrust [kN]	58.7
Takeoff thrust [kN]	254.3	Cruise TSFC [g/kN/s]	16
Takeoff BPR [-]	5.15	Cruise EGT limit [°C]	835
Takeoff OPR [-]	29.9	Cruise HP shaft speed [RPM]	9826
Takeoff TSFC [g/kN/s]	9.1	Cruise LP shaft speed [RPM]	3449
Takeoff EGT limit [°C]	960	Max HP shaft speed [RPM]	11055
Takeoff HP shaft speed [RPM]	10868	Max LP shaft speed [RPM]	3854
Takeoff LP shaft speed [RPM]	3674	Engine cost [M€]	6.1

Exhaust Gas Temperature (EGT) plays a pivotal role in monitoring and analyzing gas turbine performance. It is a critical parameter that serves as an indicator for the highest gas path temperature, which is typically found at the HPT inlet. However, due to the extremely high temperatures (around 1300 °C) in the gas stream immediately after the combustion chamber, direct measurement of the HPT inlet temperature is impractical. The instruments available are not capable of withstanding such high temperatures and would introduce significant measurement errors. In the case of dual-rotor engines, it is more common to measure the temperature between the HPT and the LPT. For GE CF6-80C2 engines, the inlet temperature of the LPT is measured and referred to as the EGT. It should be noted that actively monitoring the EGT is even more important from a safety point of view. In fact, if the temperature of the HPC blades can be controlled with the use of sophisticated cooling techniques, the same cannot be said for the LPC blades. The engineering and manufacturing costs of these meticulously designed blades are inevitably very high. Civil aviation is a very competitive sector, as highlighted by the airlines' low profit margins [46][47]. Hence, the need for airlines to keep costs low and profits high limits investments when they do not have a substantial impact on the aircraft's performance. Equipping LPTs with a cooling system is an example of this. As a result, whithout a cooling system, keeping the EGT below a certain limit is the only way to operate the LPT safely and avoid blade failures.
The difference between the actual operating temperature and the EGT limit is known as the Exhaust Gas Temperature Margin (EGT margin). In normal operation, it is advisable to maintain a minimum EGT margin to ensure an adequate overhaul interval for the engine. This is because a minimum EGT margin provides a buffer or safety margin to account for variations and unexpected conditions during operation. By keeping this margin, it helps prevent the engine from operating too close to its design limits, which could lead to accelerated wear and damage over time. Adopting a healthy EGT margin, the engine's components are less likely to be stressed excessively, promoting longevity and reducing the need for frequent overhauls and maintenance. From a review of the literature [53] and the advice provided by GE [15] it was found that maintaining an EGT margin of 50-100°C is considered a safe operating practice.

Table 2: Equivalent fuel composition

Jet A	
Atom	**Mass fraction** [-]
C	0.862
H	0.13435
O	0.00215
S	0.0015

Equivalent fuel			
Species	**Molar fraction** [-]	**MM** [kg/kmol]	**LHV** [MJ/kg]
CO	0.00185	28.0105	10.112
H_2S	0.00065	34.0799	15.2
H_2	0.24005	2.016	119.55
C	0.52917	12.011	32.763
C_2H_6	0.22828	30.0701	47.62
TOT	1	13.77811	43.1

4.2. Replacing the jet fuel with an equivalent fuel

The accurate simulation of a system involving combustion processes of one or more fuels would require knowledge of the molecular composition of the fuels used. Molecular compositions are more readily available for gaseous fuels than for liquid or solid fuels for several reasons. Gaseous fuels are easier to analyze using techniques such as mass spectrometry and gas chromatography. These techniques enable the precise determination of the chemical composition of gases. Conversely, liquid and solid fuels are more challenging to analyze as they must be converted into gas before analysis, a process that can be complex and costly. Furthermore, liquid and solid fuels can contain a wide variety of chemical compounds, making it difficult to accurately determine their molecular composition and account for them in simulation software. Atomic population and heating value are two pieces of information that are easier to obtain and vary within a narrow range, unlike the more detailed molecular composition, that is often a proprietary information and, therefore, not publicly disclosed.
Jet fuel, like other hydrocarbon fuels, is primarily composed of carbon (C) and hydrogen (H) atoms, with lesser amounts of oxygen (O) and sulfur (S). These fuels are kerosene-based and have a high energy density and high stability, making them suitable for aircraft propulsion.The exact composition and properties of jet fuels can vary, but the most commonly used jet fuel for aviation is known as Jet A. For this reason, it will serve as a reference for this discussion. The specific properties of jet fuel vary depending on the production and refining techniques employed. So, the values used are average values and serve only as an indication.
Simplification is possible and especially useful when focusing on the thermodynamic performance calculations of the overall cycle. In such cases, it is beneficial to use an equivalent fuel to simulate the behavior of the real fuel. Two fuels A and B are considered equivalent if they satisfy two conditions:

- They have the same atomic composition, meaning:

$$x_{i,A} = \left(\frac{kg_i}{kg_{comb}}\right)_A = \left(\frac{kg_i}{kg_{comb}}\right)_B = x_{i,B} \quad \forall i \qquad i = C,\, H,\, O,\, S... \tag{4.1}$$

- They have the same lower heating value LHV (or higher heating value HHV). Along with the previous condition, this ensures they also have the same higher heating value HHV (or lower heating value LHV).

Errors can arise when using this approach, and it's important to understand the situations in which it is most appropriate. The resulting compound may have a very different molecular composition compared to the real fuel, and the state of matter is not considered, neglecting latent heat of vaporization. The first condition, however, guarantees that following the combustion process, the reacted air-fuel mixture has a molecular composition identical to what the real fuel would have under complete combustion, with all hydrogen becoming H_2O, all carbon becoming CO_2, and all sulfur becoming SO_2. The assumption of complete combustion is idealized in practice, but it closely approximates the behavior of combustion processes with a large excess of air, typical of Brayton cycles. The second condition provides thermodynamic equivalence between the two systems in terms of mass flow rate of equivalent fuel and heat supplied to the thermodynamic cycle. Incomplete combustion means that the full heating value of the fuel cannot be harnessed entirely. This aspect can be accommodated by introducing a combustion efficiency η_{comb}. In conclusion, for the purposes of this research, this approach has been deemed sufficiently accurate to simulate jet fuel combustion.
The fluid that satisfies the constraints imposed was found with the use of the Excel solver [41]. There are theoretically infinite solutions to the system of equations considered given that an indefinite number of molecular species (unknowns of the system) can be added.
The reference values for Jet A [6][24][7] and the resulting equivalent fuel composition are summarized in Table 2.

4.3. Design point simulation: takeoff conditions

The following section outlines the procedure adopted for modeling the thermodynamic system giving a clear overview of the main assumptions. They are essential for interpreting the results presented in Section 5 correctly. Potential energies are neglected due to the minimal effect on the overall performance of the cycle.
The first step in creating a functional model is to understand the essential components of the real system and how they interact. To simplify the analysis and keep computational times short, only the main components have been considered, excluding secondary systems such as the lubrication circuit, the ignition system, the fuel injection system and the internal power consumption within the aircraft. These secondary systems can be added to the analysis at a later date without causing significant changes to the basic layout, and they do not have a particularly relevant impact on performance estimation. However, it should be noted that, as the measurement conditions of the available data are not known in minute detail, neglecting their effects could contribute to a difference between the model results and reference values.
The next step is to implement the resulting plant layout in a format suitable for the GS software. Inserting the components into the input file allows for easy system definition by assigning a letter of identification to each one. The definition of input and output flows for various elements is straightforward and intuitive, with the user assigning a numerical identifier to each flow. A process flow diagram of the system is shown in Fig. 10.
In addition to the bypass filter, two additional splitters have been added to perform bleeding from the core air flow before it is heated with combustion to cool the HPT stages. An iterative calculation is required to accurately estimate the coolant flow that meets the operational limits of the superalloys used for the HPT stages. In particular, two coolant flows are indicated: the first from the HPC discharge and the second upstream of the HPC. The first flow is for cooling the first stator, where high pressures, combined with coolant circuit pressure losses, require maximum available coolant pressure. The second flow is for cooling subsequent rows, where lower pressure is required to circulate the coolant. For this reason, the turbine routine considers the compression work required to bring the second flow the desired pressure, and, with user input of the compressor preceding the turbine, this work is then added to the compression work related to the primary flow.
Another additional feature that has been neglected in the model is the HPT and LPT clearance control system. In the CF6-80C2 turbofan engine, turbine clearance control is a system designed to maintain a constant gap between the turbine blades and the turbine casing over the entire temperature range in which the engine operates. The clearance control system is essential because temperature changes can cause the materials within the engine to expand or contract. If the clearance between the turbine blades and the casing isn't controlled, it can lead to issues. If there is too much clearance, it can reduce engine efficiency. On the other hand, if there is too little clearance, it can cause the turbine blades to come into contact with the casing, leading to damage and potential engine failure. Given the dynamic changes in temperature during engine operation and the resulting material deformations, active clearance control is vital to maintain engine performance, efficiency, and longevity. This active control is achieved by maintaining the turbine case temperature at the desired level using cooling flows extracted from the bypass air at the fan exit. Neglecting this feature in the model should not lead to significant errors in the performance estimation.
Once the plant layout is defined, it's essential to incorporate the constraints required for the system to function correctly. The final section of a typical GS software input file includes a dedicated part for this purpose. By

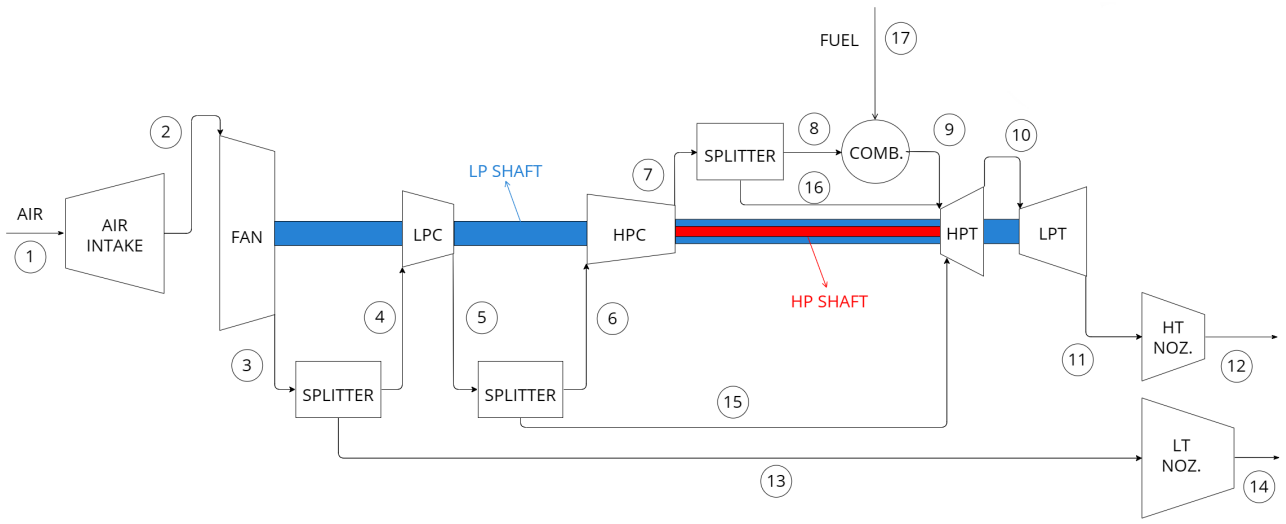

Figure 10: Process flow diagram

Table 3: Main assumptions needed for takeoff simulation

Element	Figure of merit		Element	Figure of merit	
Air intake	Total pressure ratio [-]	0.99	**HPT**	Cooled stage efficiency* [-]	0.89
Fan	Pressure ratio [-]	1.7		Mechanical efficiency [-]	0.999
	Polytropic efficiency [-]	0.891		$T_{max,blade}$ stator 1 [°C]	970
	Mechanical efficiency [-]	0.999	**LPT**	$T_{max,blade}$ rotor 1 [°C]	940
LPC	Pressure ratio [-]	2.46		$T_{max,blade}$ stator 2 [°C]	940
	Polytropic efficiency [-]	0.888		$T_{max,blade}$ rotor 2 [°C]	910
	Mechanical efficiency [-]	0.999		EGT margin [°C]	65
HPC	Pressure ratio [-]	7.15		Stage efficiency* [-]	0.92
	Polytropic efficiency [-]	0.887		Mechanical efficiency [-]	0.999
	Mechanical efficiency [-]	0.999	**HT Nozzle**	Isentropic efficiency [-]	0.98
Burner	Total pressure ratio [-]	0.98	**LT Nozzle**	Isentropic efficiency [-]	0.98
	Combustion efficiency [-]	0.994			

**This represents the efficiency of a stage under conditions of: optimal value of the specific speed and virtually infinite machine size*

differentiating variables into independent and dependent variables (a variable is independent if its value remains fixed in the input and does not change during the program's calculation; a variable is dependent if its value is determined during the calculation process), various conditions can be specified by the user indicating the desired convergence type and how variables are reassigned in each iteration. For more details on variable reassignment methods, please refer to Ref. [43]. The conditions for constraining the problem can be summarized as follows:

- **Mechanical power balance at the HP and LP shafts:** The mechanical power balance at the HP and LP shafts is a critical aspect of the system. Both shafts play a vital role in ensuring that the turbines can provide the necessary power to the compressors for processing the specified airflow at the given compression ratios, all while maintaining a fixed rotational speed and a specific number of stages. The peripheral speed of the turbines acts as a variable parameter to allow convergence. The geometry of the machine will adapt to keep the rotational speed equal to the value entered by the user.
- **Provide a suitable EGT margin:** this represents the most computationally intensive condition for the calculation program to converge. This is due to the fact that, in order to achieve the desired EGT, the algorithm must perform all the thermo-fluid-dynamic calculations related to the cooling circuits of the HPT at each iteration varying the fuel flow rate. This is essential to ensure that the blades in the four rows within it maintain a temperature lower than or at the material's maximum limit.

The key performance indices of the various components used for the takeoff simulation, are presented in Table 3 and subsequently discussed.

The fan compression ratio, β_{fan}, was chosen in accordance with the literature regarding subsonic turbofans with comparable BPR to the CF6-80C2 [39]. The remaining compression ratio, OPR/β_{fan}, which pertains to the flow passing through the engine, was divided in such a way that the isentropic enthalpy drop per stage $\Delta h_{is,st}$ was comparable between the LPC and HPC stages.

It is important to note that for a more accurate estimation of the compression ratios, it is advisable to differentiate between $\beta_{fan,bypass}$ and $\beta_{fan,core}$. In high bypass ratio fans, the flow is stratified, meaning it is divided into a bypass stream and a core stream. The pressure ratio is typically lower in the core stream than in the bypass stream due to the lower circumferential speed at the hub. The lower peripheral speed results in a reduced amount of energy transferred from the fan blades to the fluid in this region [36]. This behavior was not considered in the model by assuming β_{fan} to be the same for both the bypass and core flows. Certainly, this underestimates the compression ratios of the subsequent stages of the engine. However, since the Overall Pressure Ratio (OPR) would have remained constant, as it is a characteristic of the engine, the overall performance obtained as output would not have changed significantly.

The estimation of the dynamic inlet performance followed the guidelines provided in Section 3.2.1.

The component efficiency level is considered a technologic secret by engine manufacturers, because it represents a design capability measure of the company. For the proposal of this study, once the use of accurate values of the efficiency as an input to the engine simulation is not imperative, the component polytropic efficiencies were adopted. The theoretical concept of polytropic efficiency has advantages because it enables the comparison on the same basis for compressors/turbines of different compression/expansion ratios.

For mechanical efciencies of the low- and high-pressure spools, a value of 99.5% was adopted, according to data available in Ref.[39].

The remaining values listed in Table 3 were determined through a review of the literature combined with the

adaptation of parameters from the stationary LM6000 gas turbine. These specific numbers were selected and discussed by researchers within the Department of Energy at Politecnico di Milano as part of other projects.

4.4. Off design point: cruise conditions

Cruise conditions refer to the state in which an aircraft maintains a constant speed and altitude for an extended period of time. Unlike takeoff conditions, maximum engine performance (peak power) is not required during cruise. However, these operational conditions are of paramount importance in the design phase, often serving as the design point for some of the components involved such as turbomachinery. This is especially true in the civil aviation sector, where optimizing the overall efficiency η_o (see Appendix A.4) of the propulsion system during the majority of the flight time helps reduce operational costs associated with fuel consumption. For this reason, cruise conditions have been selected as an additional operational point for validating the model.
In this case, the engine's required thrust cannot be solely deduced from measurements or data provided in datasheets; it is also influenced by the engine-aircraft matching. Utilizing this approach to estimate the reference values for required thrust during cruise conditions offers several advantages:

- it circumvents the challenge of lacking precise information found in proprietary technical reports;
- it aligns with existing literature, providing multiple points of reference for the physical parameters involved in the estimation process;
- it provides a more comprehensive overview of the forces acting on the aircraft, allowing for further insights (Section 4.5.3).

Nevertheless, it's important to recognize that additional assumptions are needed to simplify the problem and they may also introduce the drawback of potential inaccuracies.

4.4.1 Aircraft drag estimation

During an aircraft's flight, it experiences two primary aerodynamic forces: lift and drag. Drag arises from the interaction between the aircraft's shape and the airflow, while lift results from pressure differences on the wings. In general, these lift and drag forces are expressed as functions of the wing area S, dynamic airspeed V, air density ρ, and coefficients that account for various flow effects:

$$L = C_L q S \tag{4.2}$$

$$D = C_D q S \tag{4.3}$$

where q is the dynamic pressure, defined as

$$q = \frac{1}{2}\rho V^2 \tag{4.4}$$

Accurately calculating these coefficients is challenging, as they depend on factors like the Mach number, angle of attack, boundary layer characteristics, and the aircraft's aerodynamic shape. When dealing with fixed-wing aircraft, these coefficients are often modeled as functions of the angle of attack, which measures the angle between the aircraft's body axis and the airspeed vector.
Various mathematical and experimental techniques are employed to model and predict C_L and C_D. Conducting a Computational Fluid Dynamics (CFD) simulation is a precise method for estimating these coefficients, especially when the aircraft's geometry is accurately replicated. However, developing a CFD model is time-consuming, and solving the Navier-Stokes equations computationally intensive.
For this reason, alternative approaches are sought during the initial phases of a project to quickly assess the forces involved and outline project specifications.
Focusing solely on cruise conditions has facilitated problem simplification for several reasons:

- the influence of pitch, yaw, and roll angles can be disregarded since the aircraft maintains constant altitude and does not change its flight direction, effectively reducing the system's degrees of freedom;
- during these conditions, the aircraft remains in a "clean condition," meaning significant changes in the aircraft's shape are not expected. The most notable alterations occur when employing high-lift devices (such as flaps and slats), speed brakes, and landing gear. Each of these structural settings corresponds to its own specific drag model.

The influence of these angles and other physical features exposed to the airflow becomes more significant during certain pilot maneuvers and other flight phases, such as takeoff, climbing, descent, landing, and turns.
In such simplified models, drag polar curves play a significant role in describing aircraft performance. These curves illustrate the relationship between the drag coefficient and lift coefficient, allowing to eliminate AoA dependency.

Figure 11: Boeing 747-400

Under the assumptions aforementioned and for wings with $AR > 3$ and without incorporating airfoils with extensive low drag buckets, the following parabolic drag polar equation provides a reasonably accurate curve fit for lift coefficient values ranging from 0 to 1 [45]:

$$C_D = C_{D0} + kC_L^2 \tag{4.5}$$

with:

$$k = \frac{1}{\pi AR\, e} \tag{4.6}$$

Here, C_{D0} represents the zero-lift drag coefficient, accounting for the aircraft's overall parasitic drag, while k is the lift-induced drag coefficient factor. AR is the aspect ratio of the wing (span divided by the average chord), while e is the Oswald factor, which is a correction factor that reflects the deviation from an ideal elliptical lift distribution ($e = 1$). The values of both parameters are considered as constants under a specific aerodynamic configuration of the aircraft.
Lift is essentially generated by redirecting a specific portion of the airflow downward from its original, undisturbed path. In the case of an infinite wingspan, the affected volume of air (which increases with the square of the wing span) would be infinite as well. With a uniform distribution of lift, there would be no remaining deflection angle or induced drag. However, practical aircraft have finite wing spans, and in such cases, induced drag is an inevitable consequence of generating the necessary lift to support the aircraft's weight. This phenomenon involves almost exclusively the wings since they are the ones that generate almost all of the lift This type of resistance arises from wingtip vortices and the non-uniform pressure distribution around the wings. The pressure differential between lower and upper side of a lifting wing pushes air from the high-pressure area (below the wing) to the low-pressure area (above the wing). The flow component coming from the lower side combines with the stream along the upper side of the wing tip, thus forming a sharply defined tip vortex [32]. Reduction of these two drag components can be achieved through two primary strategies.
Concerning the contribution of wingtip vortices, it can be significantly reduced by increasing the Wing Aspect Ratio (AR), adopting longer and thinner wings.
Regarding the second component, which is the non-uniform pressure distribution around the wings, this can be markedly reduced by increasing the Oswald Efficiency Factor e. For subsonic commercial aicrafts e lies typically in the range 0.7-0.9 and can be enhanced by features such as tip-tanks and winglets [32]. A higher e signifies a wing with a more aerodynamically efficient profile.
The objective of this article is not to delve into a detailed discussion of the nature of these losses, but an overview was necessary to give the reader a good contextualization; for an in-depth understanding, it is advisable to refer to aerodynamics textbooks and specific research papers like the ones in Ref. [45][32][48][28][30].
The aircraft selected for this study is the Boeing 747-400, whose side view is shown in Fig. 11. This model has been widely employed by major global airlines since its introduction to the market. The 747 held the world record for passenger capacity for 37 years [8]. In the passenger version (747-400), it can accommodate 416 passengers with a typical three-class configuration [9]. The primary reason for choosing this aircraft is that a subset of these planes is equipped with 4 CF6-80C2 engines, which are the reference engines considered in this study.
The lift coefficient C_L can be determined by balancing the forces acting in the direction parallel to the weight force and perpendicular to the motion as expressed in the following equation:

$$C_L = \frac{2mg}{\rho V^2 S} \tag{4.7}$$

The mass used in this calculation should closely approximate the actual mass of the aircraft in cruise conditions. To the operating empty weight (OEW) of the aircraft, we need to add the weight of cargo and passengers (total payload). For the weight of the carried fuel, an arithmetic mean between a full tank and a tank with a 15%

fuel reserve has been considered. This is because in the event of an inability to land or the need to divert to other airports, this reserve is essential. The use of an average value is a probabilistic assumption, as in cruise conditions, the aircraft typically experiences a weight in that vicinity for most of the time.
The calculation of the remaining parameters C_{D0} and k is required to define the drag polar. For this specific aircraft and other models a study was conducted by Junzi Sun, Joost Ellerbroek, and Jacco Hoekstra [48] using a stochastic total energy model to predict the drag polar. The results were then validated through CFD simulations. The resulting drag polar is depicted in Fig. 12a.
Finally, the last drag contribution to consider is the wave drag, relevant at high Mach numbers. When the aircraft operates at high Mach numbers, it's crucial to account for the effects of airflow compressibility. In these conditions, drag can significantly increase due to local supersonic flows and the formation of shock waves.
To model this phenomenon, the critical Mach number M_{crit} has to be evaluated. The critical Mach number represents the lowest Mach number at which any part of the aircraft experiences airflow at the speed of sound. This critical Mach number is often related to the drag divergence Mach number M_{dd}, which signifies the Mach number at which drag starts to rapidly increase with the aircraft's speed.
The calculation procedure for these two values is detailed in the work conducted by Hoekstra et al. [48] (which is the same procedure adopted by Filippone in his work [28]), obtaining specific values for the Boeing 747-400 aircraft.
Finally, as described by Gur et al. [30], the increase in the zero-lift drag coefficient caused by wave drag $\Delta C_{D0,w}$ is formulated as follows:

$$\Delta C_{D0,w} = \begin{cases} 0 & \text{if } M \leq M_{crit} \\ 20(M - M_{crit})^4 & \text{if } M > M_{crit} \end{cases} \tag{4.8}$$

At this point the total zero-lift drag coefficient can be reformulated as:

$$C_{D0,tot} = C_{D0} + \Delta C_{D0,w} \tag{4.9}$$

Once M_{crit} is exceeded, the rapid and non-linear increase in drag causes strong penalties because the formation of shock waves caused by the presence of transonic and supersonic flows becomes more frequent. The first areas where these conditions are established are the suction sides of airfoils such as the wings and blades of turbomachines, where the pressure is low and the air speed is high. This trend can be recognized in Fig. 12b where polars at different flight Mach numbers are illustrated.

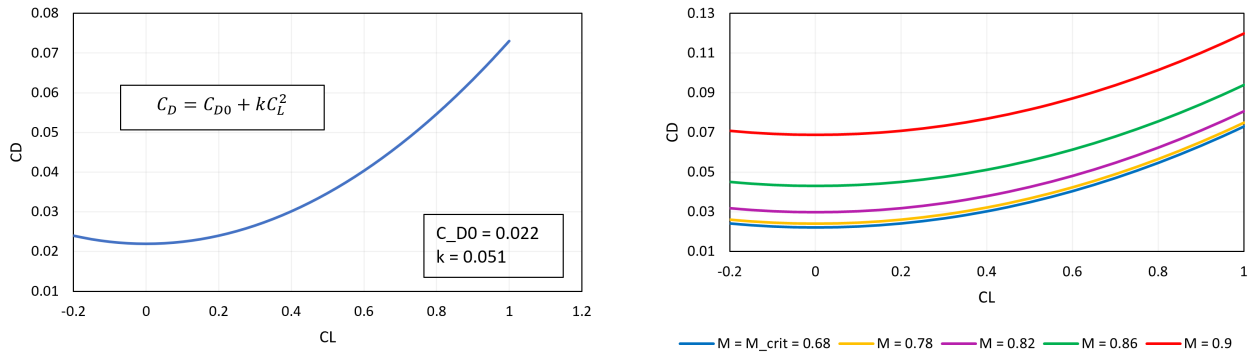

(a) *Clean configuration* (b) *Mach number influence*

Figure 12: Boeing 747-400 drag polars

4.4.2 Off-design behavior of the system

Turbomachinery (passage areas, blade geometry), heat exchangers (passage areas, heat exchange surface) and all the other components are sized under average operating conditions. If any of the boundary condition changes, the system reacts by adapting and finding a new operating set-up.
The off-design analysis of a complex system is undeniably a challenging endeavor, often requiring a detailed examination. It's important to note that the objective of this study is not to achieve extremely precise results. There are two primary reasons for this: firstly, the scarcity of reliable data for direct comparison, and secondly, the inherent uncertainties introduced by the assumptions and simplifications made.
Instead, the aim of this analysis is to obtain reference values that are approximately correct. It also seeks to provide a qualitatively accurate estimation of the variations in turbomachinery efficiencies, which are the central focus of the thermodynamic simulation.

Correctly describing the behavior of turbomachinery is a fundamental and considerable part of off-design analysis of a turbofan engine. If the working fluid is incompressible, as in the case of pumps, it can be applied with excellent approximation of the theory of similarity and obtain generalized maps of operation. On the other hand, if the fluid is compressible, the theory of similarity has some limits of applicability, but it's still usable. In this case, the variables to use are:

- dimensionless reduced flow rate (or corrected, always referring to the inlet of the machine)

$$\dot{m}_r = \frac{\dot{m}_{in}\sqrt{\frac{R}{MM}T_{in}}}{p_{in}A_0} \tag{4.10}$$

- dimensionless reduced speed (or corrected)

$$\frac{RPS\, D_0}{\sqrt{\frac{R}{MM}T_{in}}} \tag{4.11}$$

- compression (or expansion) ratio β
- isentropic (or polytropic) component efficiency

where A_0 and D_0 are respectively suitable reference area and suitable characteristic diameter that serve to dimensionless the magnitude and whose values are arbitrary.

The mass flow rate of air ingested by the engine can be approximated quite well: while the volumetric flow rate decreases slightly ($\approx 5\%$) compared to the case of peak take-off load, a significant influence is due to the variation of the air density with altitude. In fact, at an altitude of 10500 m the density is reduced by about a factor of 3.15.
The speeds of the HP and LP shafts are considered to be known from the indications provided by the manufacturer in Ref.[15]. They are presented in Table 1.
On the contrary, there is no indication of changes in compression and expansion ratios. To overcome this drawback, geometrical and thermo-fluid dynamic considerations have made it possible to indirectly find the new operating point by imposing the following constraints:

- at a fixed rotational speed, in order to keep the geometry unchanged from the design case, the peripheral speed of the turbines must be adjusted accordingly;
- the balance of the HP and LP shafts was originally controlled by varying the geometry of the respective turbine. In this case, the peripheral speed is determined by the previous condition. It was chosen to use the isentropic load factor as a free parameter to achieve convergence. Velocity triangles will vary a little bit, changing the turbine specific enthalpy drop;
- the passage areas of the HPT cooling circuits must be kept unchanged. These circuits are rarely equipped with actively controlled valves, so the circulating flow rate will be determined by the pressure difference between inlet and outlet. The temperature of the metal at this point will adapt, resulting lower at partial loads as the coolant will be excessive;
- the radiative thermal losses from the hot parts of the engine will remain almost constant as they depend almost exclusively on the temperatures of the materials, which vary very weakly;
- reduced flow rate above a certain expansion ratio value is blocked. For many applications, the expansion ratio accross the turbine is high enough to be able to consider the constant reduced flow rate with a good approximation. The turbines then work generally in sonic block, and the expansion ratio variation does not result in any variation of the reduced range. Varying β_{HPC} and β_{LPC} allows this pattern to be mathematically reproduced. Unfortunately there are two conditions for three compressors, so β_{fan} must be imposed by the user. A serious mistake cannot be made by placing the compression ratio around 1.7.

In the absence of component maps, efficiencies must be defined by the user in GS. In general, moving from takeoff conditions to cruise conditions, efficiencies increase slightly. For the fan and booster, a variation of 1.5% was chosen, while for HPC a 0.75% was deemed sufficient. The reason is that CF6-80C2 HPC is equipped with 5 VGVs, dedicated to modulating the flow rate while maintaining high efficiency. On the other hand, it is possible to consider the efficiency of the two turbines constant for the choked flow condition mentioned above. The results of the analysis conducted with GasTurb software [5] (Appendix B) and discussions with highly qualified professionals in the university environment [10] provided a higher level of reliability to the values used.

4.5. Implementation of the hydrogen system

After validating the new components, the conventional jet fuel was replaced with hydrogen. A novel design configuration was then explored, involving the cooling of high-pressure turbine cooling flows (hot fluid) with the cryogenic hydrogen flow exiting the tank (cold fluid). In these conditions, the heat required to heat up the

fuel flow is supplied by the cooling flows intended to cool the first stage of the high-pressure turbine, thereby reducing their temperature. This, in principle, should allow for a more efficient engine operation through the rational use of heat. Colder flows for turbine blade cooling should have a dual positive effect, both deriving from the reduction in mass flow of these flows:

1. with the same amount of air ingested by the engine, it reduces the fraction of air processed by the compressor that does not enter the combustion chamber (which is a source of loss as it does not follow the classical Joule-Brayton cycle path);
2. it reduces the fluid-dynamic irreversibilities of the open-cycle 'film cooling' process resulting in minor flow disruption due to injection of coolant, consequently leading to an increase in efficiency. According to Brewer [20], the efficiency penalty schedule used should impose a reduction of aboout 0.2 points of efficiency for each percent of total airflow used as coolant. However, estimating the real effect on efficiency is quite hard because many thermo-fluid-dynamic processes are involved. For this reason, it was chosen not to account for this expected improvement in efficiency, slightly underestimating all the benefits related to this configuration.

Subsequently, the plant layout was changed again to evaluate the effect of an additional cooling process: a compressor air intercooling.
An additional benefit is the fuel pre-heating effect. Normally, part of the heat released in the combustion process is required to heat the fuel to compressor discharge temperature. The increase in temperature of the fuel at the heat exchanger outlet minimizes this penalty. The concept of regenerative fuel heating becomes particularly relevant in the case of LH_2 because of the negative effect on cycle efficiency of introducing low temperature fuel at the combustor inlet. As noted by Brewer [20], the introduction of low temperature fuel into the combustor results in a performance penalty when compared with the fuel temperatures typical of conventional kerosine-type fuels.

One essential metric in aircraft design is the thrust-specific fuel consumption (TSFC) of the engine, which is the fuel mass flow rate required per unit thrust the engine produces, as defined in A.5. Although TSFC is widely used for comparing engines, it is not appropriate for comparing engines that use fuels with different energy densities. For example, a given mass flow rate of hydrogen delivers nearly three times more energy than the same mass flow of kerosene. Instead of quantifying the mass flow rate per unit thrust, it is more appropriate to quantify the energy consumption per unit thrust. This leads to the thrust-specific energy consumption (TSEC) involving the lower heating value of the fuel (120 MJ/kg for hydrogen and 43 MJ/kg for kerosene), which is written as:

$$TSEC = TSFC \cdot LHV \tag{4.12}$$

4.5.1 Preliminary considerations

Since the extremely low temperatures (T $<$ 150 K) of the hydrogen stream in the real system would have introduced significant inaccuracies when calculating the thermodynamic properties of the hydrogen stream using the GS software, specific enthalpy values were calculated using REFPROP [38] and then manually entered into the simulation program. Molecular hydrogen occurs in two isomeric forms, one with its two proton nuclear spins aligned parallel (ortho-hydrogen), the other with its two proton spins aligned antiparallel (para-hydrogen) [16]. Para-hydrogen is in a lower energy state than is ortho-hydrogen. At room temperature and thermal equilibrium, thermal excitation causes hydrogen to consist of approximately 75% ortho-hydrogen and 25% para-hydrogen and it is known as "normal hydrogen". When hydrogen is liquified at temperatures below 180 K, there is a slow spontaneous transition to a predominantly para ratio, with release of energy. Essentially pure para-hydrogen form can be obtained at very low temperatures. This shift impacts the calculation of thermodynamic properties, leading to deviations in specific heat of up to 20-30%. The actual composition depends on the kinetics of these internal reactions, but it is reasonable to assume an equilibrium condition for our calculations. By default, REFPROP includes only the normal form of hydrogen. It was manually integrated with an equilibrium dataset based on studies carried out by Le Roy et al. [37].

4.5.2 Modification of the thermodynamic cycle

Two heat exchangers "HX 1" and "HX 2"operating with a user-defined specific enthalpy drop for the hydrogen stream was added to the basic configuration in Fig. 10. The modified plant layout is reported in Fig. 14.
Flow 19 corresponds to cryogenic pump outlet conditions. Pumping LH_2 right at tank outlet allows to minimize electrical consumption because the fluid density is maximum.
Flow 17 and flow 5 are now able to heat up the hydrogen and and in the meantime lower their temperature. The analysis was conducted for increasing values of fuel specific enthalpy drop. Under the simplifying assumption that the weight and the external shape of the aircraft remains almost unchanged, the requested thrust will be the same as the jetfuel case. For this reason, the hydrogen case without cooling was selected for the choice of

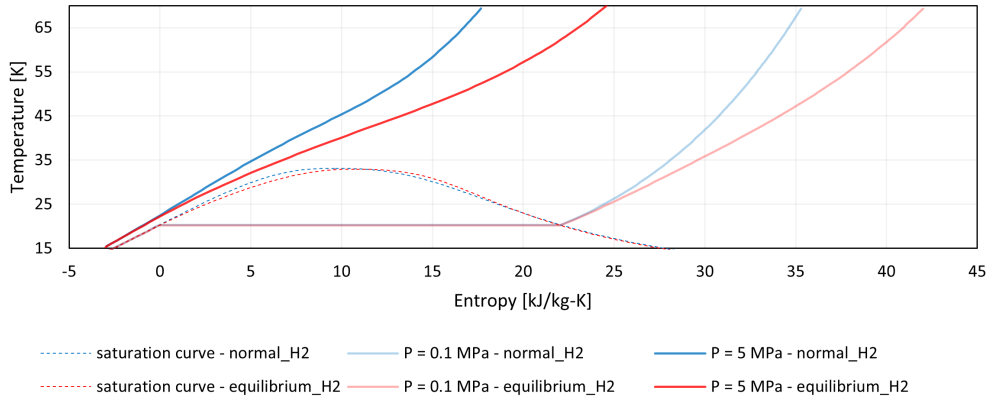

Figure 13: T-s diagram for normal hydrogen

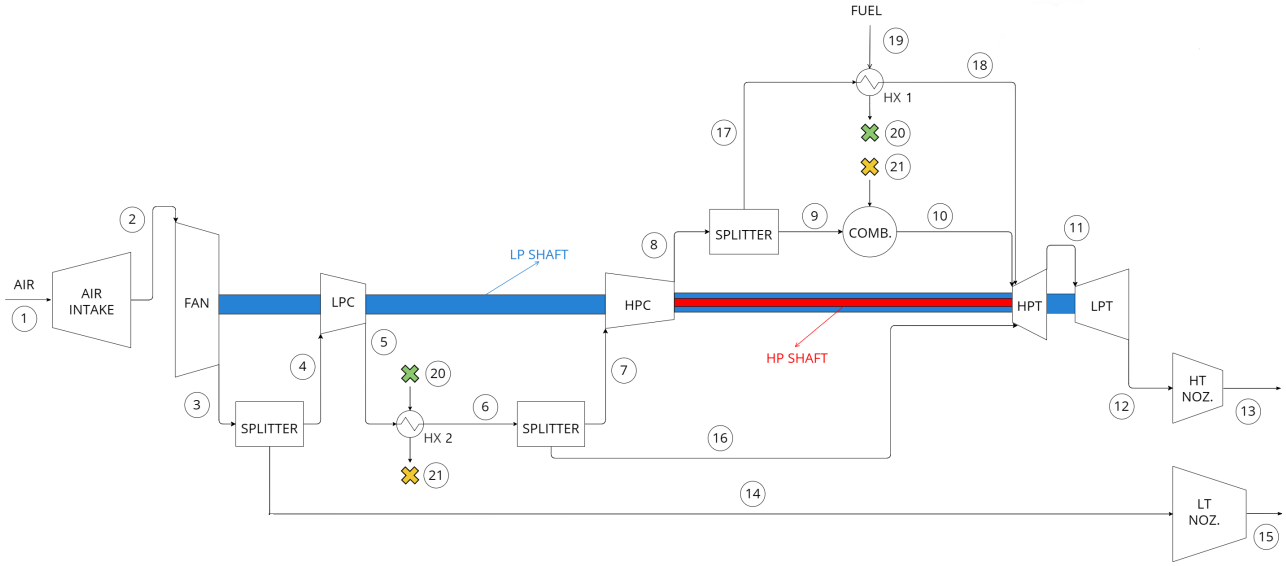

Figure 14: Process flow diagram

the reference thrust value. For all cycle investigations, compressors' pressure ratios, ingested airflow and BPR were held constant to be consistent with the operating parameters of the reference engine. Accordingly, TIT will adjust to meet the thrust requirement.
The temperature and pressure of the fuel flow 17 were arbitrarily chosen in GS and kept constant for all simulations. Although the absolute values of the specific consumption depend on this arbitrary choice, the percentage variations of this parameter in this parametric study are not or only weakly influenced in the case of a unique choice for all simulations.

Cooling of turbine cooling-air The LH_2 stream is characterized by a high specific heat and very low temperatures, resulting in a high cooling power. Conversely, the low mass flow rate and poor heat exchange capacity of turbine cooling-air (flow 16) tend to rise in temperature quickly, limiting the full exploitation of the cooling benefits. To maximize the amount of heat exchanged, a modification to the cooling flow configuration was made compared to the baseline case described in Section 4.3. Flow 16 in Fig. 10 was originally intended for cooling only the first stator of the HPT. By comparing the estimated temperature drop of the relatively low mass flow in flow 16 with the required enthalpy increase (as an order of magnitude), it was decided to also assign the cooling of the first rotor of the HPT to flow 16. The spillage pressure of the flow required by the first rotor was originally equal to the cycle's maximum, so no efficiency penalties due to over-pressurization are expected. This will result in an increase in heat exchanged for the same air temperature drop.
Pressure drops were neglected for both the fluids in this study for simplicity because they are function of the exchanged heat and it is a varying parameter.

Compressor intercooling Positioning a compressor intercooler in a turbofan configuration requires careful considerations. In general, achieving the same pressure ratio with a higher fluid density leads to lower power consumption of the compressor and to a reduction in size and weight of rotating machines. From a thermodynamic point of view, increasing the air density as soon as possible is advisable to get the maximum advantage. Basically, an intercooler right before the fan would benefit both the fan, the booster and the HPC. However, a technical-economic feasibility analysis highlights the drawbacks in terms of added weight of this concept. Operating with lower air-fuel temperature difference, typical of a intercooler preceding the fan, would result in higher heat exchange surfaces and could cause a severe air-side freezing problems. For this reason a more conservative solution was considered, palcing the intercooler right before the booster compressor.

4.5.3 Additional Considerations

It is necessary to clarify that the modification to the conventional system involves a change in the weight of the propulsion system due to the presence of a heavy tank and the addition of a heat exchanger. On the other hand, the marked reduction in the weight of the fuel transported due to the high calorific value of hydrogen should be considered.
However, a complete analysis cannot be limited to considering only the components related to the engine, but must also take into account the entire structure of the aircraft.
Hydrogen-fueled aircraft typically exhibit a marginally lower lift-to-drag ratio (L/D) and a reduced wing loading (gross weight/wing area) compared to conventionally fueled counterparts. These characteristics stem primarily from the comparatively low density of hydrogen fuel.
The reduced L/D arises from the fact that while requiring about one-third the weight of jet fuel, liquid hydrogen (LH2) demands significantly more volume. It is advantageous to store LH2 within the fuselage instead of wing tanks, as is common practice with jet fuel, to minimize the surface-to-volume ratio of the storage tanks. Consequently, LH2-fueled aircraft tend to possess larger fuselages. Additionally, due to the lighter fuel weight, LH2-powered designs generally have a lower takeoff weight compared to jet-fueled counterparts, necessitating less wing area for takeoff from a given runway length. This combination of a larger fuselage and a smaller wing naturally translates to a lower L/D.
The lower wing loading characteristic derives from the fact that LH2-fueled aircraft experience an abnormally low fuel burnoff rate during flight. To maintain equivalent landing distance capability, the wing loading at landing should remain comparable to conventionally fueled designs. Therefore, the wing loading at takeoff will always be lower for LH2-fueled aircraft compared to their jet-fueled counterparts.
It is clear at this point how the detailed thermodynamic analysis must necessarily be carried out in parallel with the design of the aircraft as the overall weight has an influence on the requirements of the propulsion system in terms of thrust and specific consumption. This is beyond the scope of this study.

5. Results & Discussion

5.1. Conventional cycle validation

The chosen validation process involves comparing the most important performance parameters for a jet engine with the reference parameters for the motor in question. There are two main figures of merit: thrust (Appendix A.1) and thrust specific fuel consumption (Appendix A.5). Physical properties in correspondence of the thermodynamic stations are not reported due to the absence of terms of comparison. However, substantial differences with the actual engine are not expected in case thrust and TSFC meet the requirements.
Table 4 and Fig. 15 show the absolute values and the deviations for this quantities respectively for the particular reference engine chosen and in general compared to the values of jet engines found in the literature.

Table 4: Results obtained versus expected results

	Takeoff			Cruise		
	Data	GS	Deviation	Data	GS	Deviation
Thrust [kN]	254.26	260.68	2.46%	54.01	53.55	-0.85%
TSFC [g/kN/s]	9.2	9.681	4.97%	15.98	15.42	-3.50%

Looking at Fig. 15, it is appreciable how the qualitative trend of specific thrust and specific fuel consumption is faithfully reproduced by the simulations conducted in GS. In addition, the two operating points approximate quite well the typical behavior of a high bypass ratio turbofan engine. In this context, it's worth recalling why those curves have that particular shape to understand what physical behaviors the program is now able to

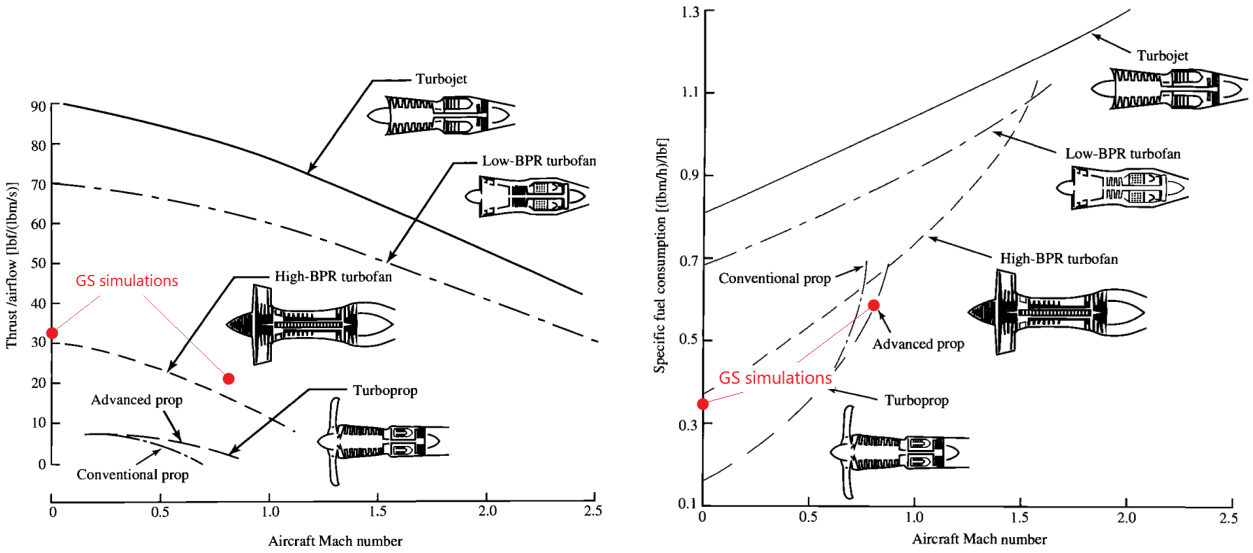

(a) *Specific thrust characteristics of typical aircraft engines*

(b) *Thrust-specific fuel consumption characteristics of typical aircraft engines*

Figure 15: Comparison with literature [39] - main figures of merit

capture. As altitude rises, the reduced air density means less airflow ingested by the engine, causing less thrust to be created. The bypass ratio does not change, so the core airflow also decreases by the same amount as fan airflow. So fuel flow should be decreasing too! So why is the TSFC twice as bad for cruise as takeoff? Because the entry impulse goes up while the exit impulse stays roughly constant. Thrust is the difference between both, derived over time. The moving engine needs to slow down the airflow for combustion to take place, and then needs to accelerate the air by more than it has been slowed down to have positive thrust. While the internal process inside the engine in flight is very similar to that at rest (only the pressure levels are increased by the ram effect of the moving engine and density drops with increasing altitude), thrust is reduced due to the smaller impulse difference in flight. Since a high bypass ratio engine accelerates most of the air volume flowing through the fan by only a little, the average exit speed is relatively low compared to a jet engine with no bypass flow. In other words, thrust tends to decrease more rapidly both then fuel consumption and airflow. SFC gets even worse in supersonic flight. That is the reason why for a meaningful SFC comparison flight speed needs to be the same.

Both the comparison with literature and with the CF6-80C2 reference values highlight relatively small deviations for the engine simulated in GS. Looking at takeoff conditions in [table sopra], the CF6-80C2 reference TSFC is about 5% lower than the one calculated. This deviation it is not irrelevant and deserves attention. The fact that the GS resulting thrust is also higher gives a warning about the EGT margin assumption. A lower EGT margin determines a higher TIT and therefore higher thrust and higher fuel consumption. However, thrust deviation is roughly one half of TSFC deviation. It suggests first that the TSFC inaccuracy can be mainly attributed to the fuel mass flow rate estimation. Here, the actual lower heating value of the jetfuel has direct implications, causing additional uncertainty on the calculation. Secondly, it's right to consider that the CF6-80C2 reference TSFC comes from General Electric's public sources for promotional purposes, which often do not reflect real values.

Having imposed the EGT margin, a further check can be made by comparing the TIT values with the maximum values proposed by Mattingly [39]. Selecting the level of technology that most likely matches that of the CF6-80C2 (the levels of technology can be thought of as representing the technical capability for 20-yr increments in time beginning in 1945. Thus level 3 of technology in this case presents typical component design values for the time period 1985-2005), it can be appreciated that at take-off, the condition characterized by the highest thermal stresses, the GS resulting TIT = $1507\,°C$ is very close to the indication provided by the book, while still remaining below.

Regarding cruise operation, thrust seems to be not far from the reference value. However, it must be kept in mind that the reference value is equal to the aircraft drag estimation carried out by the author. TSFC is instead taken from the online dataset related to the book written by Jenkinson et al. [33]. Since the two sources are very different, different deviations can be expected between the two figures of merit. The simplified off-design model used contributes to provide less reliable results.

At the end of the day, considering the large number of parameters involved in a turbofan engine, the neglected

phenomena and the suboptimal quality of the data on the reference engine available, the model can be considered validated. Any modifications necessary to adapt the code to other types of jet engines can be made without particular problems given the modular nature of the GS code.

5.2. Hydrogen as fuel

The results provided by the software in the case of hydrogen-powered turbofans aim to evaluate possible improvements and highlight possible critical issues arising from fuel replacement. All comparisons in this section are made under takeoff conditions. At higher power, more deviations are expected, making the advantages and disadvantages of fuel replacement more appreciable. However, in Section 5.2.2 heat exchangers will be introduced compared to the original configuration: in cruise conditions lower air temperatures are expected. At the same temperature of the hydrogen extracted from the tank, the temperature differences in the exchangers will inevitably be different than in the case of sea level. Specific considerations regarding the off-design of these components must be made in order to obtain significant results. This is beyond the scope of this report.

5.2.1 Effects of fluid composition variation

The first analysis conducted with hydrogen considers only the substitution of the fuel and does not include any variation to the thermodynamic cycle, neither in terms of plant layout nor in terms of temperatures and pressures of the incoming flows. The simulation was performed as a design point. It means that the geometry will vary to accommodate the design parameters given in input. Therefore, it must be said that this comparison serves as an indication to generally understand the effect of burning hydrogen in a turbofan engine. If the goal is to replace the fuel and use the existing engine unchanged a comprehensive analysis including off-design considerations must be carried out. A useful guide for this purpose and a good accompaniment to the analysis reported below can be found in Ref. [12] and Ref. [21].
The results are reported in Table 5.

Table 5: Main cycle parameters variation

	JETFUEL	**H2 (1)**	**Deviation**	**H2 (2)**	**Deviation**
Thrust [kN]	260.68	268.32	2.93%	260.68	0.00%
TSEC [kW/kN]	412.3138	417.16	1.18%	403.82367	-2.06%
Core jet velocity [m/s]	446.94	511.47	14.44%	446.94	0.00%
TIT [°C]	1507	1507	0.00%	1466	-2.72%
Δh_{is} stage 1 HPT [kJ/kg]	239.75	243.38	1.51%	241.48	0.72%
Δh_{is} stage 2 HPT [kJ/kg]	234.75	238.3	1.51%	236.44	0.72%
$T_{tot,out}$ HPT [°C]	894.9	902.7	0.87%	865	-3.34%
$P_{tot,out}$ HPT [bar]	8.78	9.15	4.21%	8.86	0.91%
Δh_{is} stage 1 LPT [kJ/kg]	87.011	88.121	1.28%	88.149	1.31%
Δh_{is} stage 2 LPT [kJ/kg]	91.985	93.158	1.28%	93.187	1.31%
Δh_{is} stage 3 LPT [kJ/kg]	96.644	97.876	1.27%	97.907	1.31%
Δh_{is} stage 4 LPT [kJ/kg]	100.94	102.23	1.28%	102.26	1.31%
Δh_{is} stage 5 LPT [kJ/kg]	104.82	106.15	1.27%	106.19	1.31%
$T_{tot,out}$ LPT [°C]	527.5	544.5	3.22%	502.6	-4.72%
$P_{tot,out}$ LPT [bar]	1.62	1.81	11.73%	1.62	0.62%
$MM_{out,comb}$ [g/mol]	28.983	27.645	-4.62%	27.734	-4.31%
$\overline{c_p}$ LPT [kJ/kg/K]	1.171	1.216	3.83%	1.202	2.64%
$\overline{h}$ stator 1 HPT [kW/m2K]	5.81	5.896	1.49%	5.894	1.45%
ΔT_{TBC} stator 1 HPT [°C]	141.07	142	0.66%	119.65	-15.18%
ΔT_{blade} stator 1 HPT [°C]	80.61	81.15	0.66%	68.375	-15.18%
$\dot{m}_{cool}$ [kg/s]	8.1623	8.4181	3.13%	6.938	-15.00%
$\dot{m}_{in}$ LPT [kg/s]	130.97	129.38	-1.21%	129.33	-1.25%
$\dot{V}_{in}$ HPT) [m3/s]	19.48	20.16	3.50%	18.469	-5.17%
$\dot{V}_{in}$ LPT [m3/s]	49.99	49.88	-0.23%	49.714	-0.55%

The propulsive thrust increases by 2.93%, mainly driven by a different fluid composition flowing through the turbine. The higher water content leads to a higher average specific volume of the working fluid, allowing to

have the same power output with a lower expansion ratio. This "pressure recovery" can be exploited at the core nozzle. This overall thrust improvement is expected to be higher for lower bypass ratios and of course for jet engines, where the core nozzle accounts for a more significant portion of the total thrust.
The resulting TSEC increases by 1.18% in case of the same TIT. Increasing the temperature of the products of hydrogen combustion requires more energy than in the conventional case due to high specific heat of water vapor. To better explain the effects on fuel consumption, it is more correct to refer to a case with the same thrust. A further simulation varying TIT showed that a TIT reduction of 41°C allows to have the same thrust of 260.68 kN with a reduction of TSEC of 2.06%.
The enthalpy drop Δh increases in both the HPT and in the LPT for every stage by approximately 1.5%. For an ideal gas (as the engine exhaust are considered in GS), the isentropic enthalpy drop can be evaluated through the expression

$$\Delta h_{is} = \int_{T_{in}}^{T_{out,is}} c_p(T)dT = \overline{c_p}(T_{out,is} - T_{in}) \tag{5.1}$$

Higher water content enhances the mixture's specific heat but concurrently reduces the isentropic exponent, leading to a diminished temperature drop and, consequently, an increased turbine outlet temperature. This reduces the EGT margin maintaining the same TIT. The required Δh to drive the compressors remains the same, resulting in lower turbine pressure ratios. Outlet conditions of the LPT are more influenced because the expansion occurs twice.
Replacing the havier CO_2 molecules with the lighter molecules of H_2O leads to a 4.62% reduction in exhaust molar mass $MM_{out,comb}$.
The high specific heat has also influence on the average heat transfer coefficient, promoting the heat transfer between the exhaust bulk phase and the cooling circuit. The temperature drop accross the blade material and the external thermal barrier coating slightly increases, while the coolant mass flow has to rise in order to keep the blades of the HPT turbine under the temperature limit.
As expected, the exhaust mass flow rate is lower due to the high calorific value of hydrogen, even considering the coolant mass flow. Conversely, the volumetric flow rate increases by 3.5% due to high fuel volumetric flow rate and lower exhaust molar mass. At the LPT inlet the deviation tends to vanish because the pressure is higher in the case of hydrogen combustion.

5.2.2 Evaluation of liquid hydrogen cooling capabilities

The results presented in Fig. 16 make it possible to evaluate the combined effects of the two cooling methods used and, at the same time, to distinguish and compare the effects of each of them.
The analysis was conducted for various hydrogen specific enthalpy drops, ranging from 0 up to a value of 4500 kJ/kg. All comparisons will be made against the hydrogen case without cooling ($\Delta h_{HX1} = 0\,kJ/kg$). Initially, the hydrogen is heated by the turbine cooling air only in the HX 1 heat exchanger. Above 1750 kJ/kg, the temperature drop of the turbine cooling air would exceed 450 °C and therefore, from then on, further heat exchanges must be made in the HX 2, where hydrogen cools the core flow coming out of the booster compressor.
Clearly, hydrogen temperature has an almost linear trend in Fig. 16a. The imperfect linearity is given by the variation of the specific heat with the temperature. Hydrogen enters HX 1 in supercritical conditions ($P \approx 50\,bar$). The heating process requires the passage close to critical conditions where the effects of real gas are not negligible. While for a subcritical transformation the phase transition is isothermal and therefore the specific heat tends to infinity, in supercritical conditions the temperature does not remain constant, but the specific heat still has a peak of high value near the critical temperature.
Interesting notes can be written looking at Fig. 16b and Fig. 16c. As anticipated, the temperature of HPT cooling air drops rapidly in the range 0-1750 kJ/kg. When HX 2 starts to work as well, both inlet and outlet temperatures are affected. However, the outlet temperature decreases more than the inlet one because the coolant has a lower flow rate. In fact, to keep the blade material below the limit temperature with a lower TIT, less coolant flow rate is required, especially if it is tapped at a lower HPC outlet temperature. This aspect highlights how reversing the order of the two exchangers along the hydrogen circuit could be beneficial because the use of an intercooler brings both classical advantages in compressor work and a reduction in HPT coolant flow rate.
As expected, to keep the same engine thrust with improved thermodynamics, TIT will gradually decrease (Fig. 16d). Thus, less H_2 is needed in the combustion chamber. This is the direct driver of TSEC reduction (Fig. 16f). The marked difference between the TSEC trends of the 0-1750 kJ/kg range and the 2000-4500 kJ/kg range still highlights the different effectiveness of the two cooling methods: while adding HX 1 helps reduce TSEC by 0.34% for a $\Delta h_{HX1} = 1750\,kJ/kg$, the HX 2 intercooler allows an additional 1.84% reduction for a $\Delta h_{HX2} = 2750\,kJ/kg$.
As TIT decreases, the thermal power to be extracted by the HPT coolant decreases, which causes a decrease in the temperature jump over the blade materials. As visible in Fig. 16e, there is a smaller temperature difference

accross the TBC and accross the blade. Under these conditions, the material is subjected to lower thermal expansion and compression stresses. In particular, the thermal expansion coefficient of the TBC is lower than that of the metal on which it is laid. This, under the most critical operating conditions, can lead to cracking of the TBC negating its benefit. Hence, this trend would help the turbine blades to operate in safer conditions. The benefit to be realized is limited in a real application by the effectiveness and the air side pressure drop of the heat exchangers.

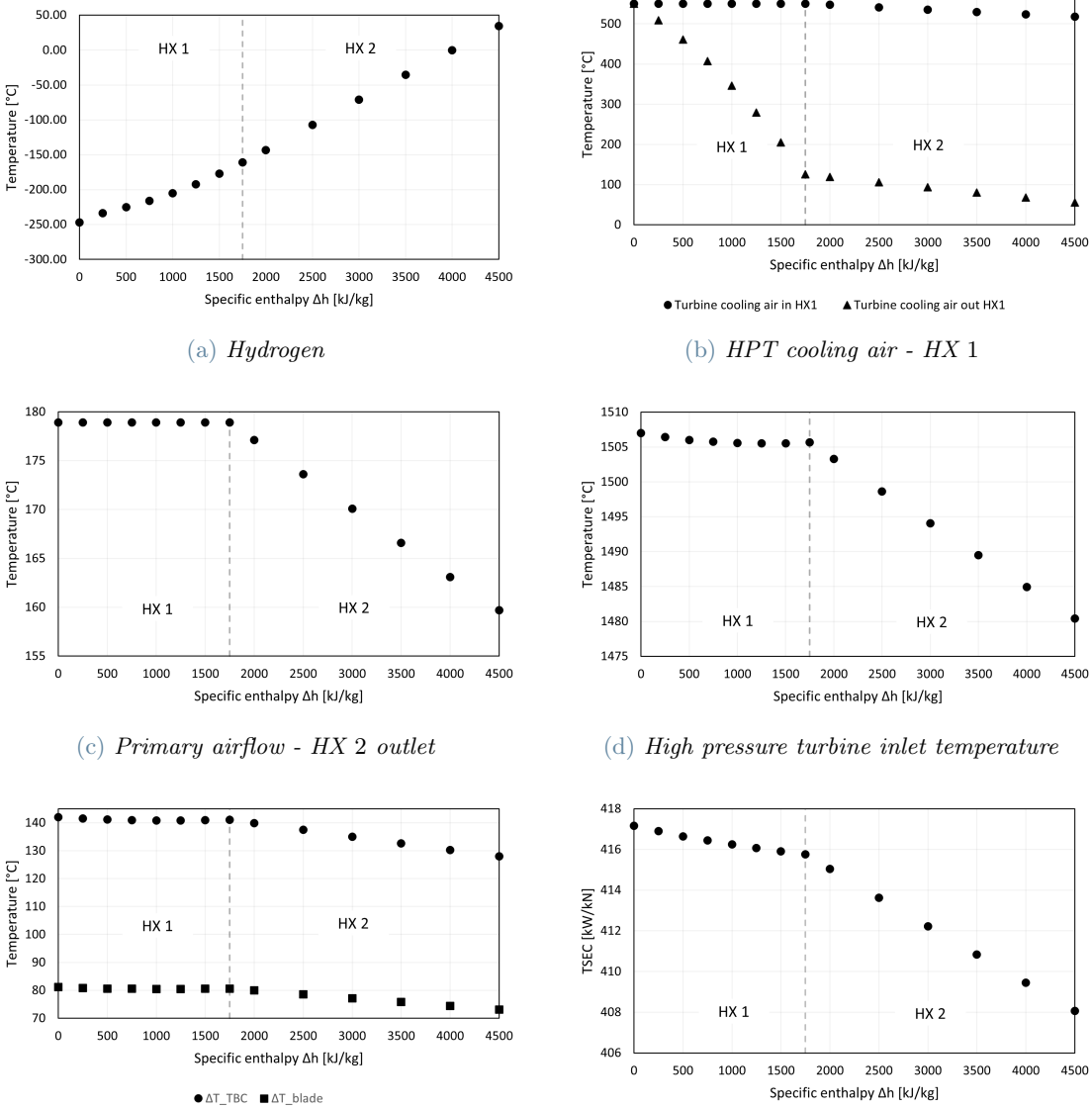

(a) *Hydrogen*

(b) *HPT cooling air - HX* 1

(c) *Primary airflow - HX* 2 *outlet*

(d) *High pressure turbine inlet temperature*

(e) *TBC and blade temperature drops*

(f) *Thrust specific energy consumption*

Figure 16: Specific enthalpy parametric study results

6. Conclusions & Possible future developments

The modeling of the nozzle and intake components has empowered our in-house software to assess the thermodynamic performance of jet engines at different altitudes and flight speeds. The integration of the developed algorithms with existing routines has proven satisfactory. Model calculations and underlying assumptions have been validated by replicating the operation of the actual GE CF6-80C2 engine and comparing the results with its specifications (target data). The identified discrepancies are minor and have been primarily attributed to inaccuracies in reference data. Further validation through a literature comparison has enhanced the reliability of the model. The study has focused on analyzing subsonic flight conditions and jet speeds up to sonic levels, guided by the concentration on a turbofan engine typically designed for operations within these conditions, a common choice for civil aviation applications.

Expanding the program's capabilities to simulate supersonic flights would open avenues for various applications, where the cooling abilities and high laminar flame speed of hydrogen play a crucial role.
The straightforward replacement of conventional jet fuel with hydrogen has highlighted the superior properties of water-rich combustion exhausts, resulting in an approximately 2% improvement in thrust-specific energy consumption. Moreover, by harnessing the cooling potential of liquid hydrogen, an additional reduction of approximately 2% in thrust-specific energy consumption can be achieved. Heat sources include the cooling flows from the hot zones of the gas turbine and the core airflow. Two heat exchangers downstream of the high-pressure compressor and downstream of the booster compressor (intercooler) has been used for this purpose. In both cases, reducing the maximum cycle temperature ensures the same thrust output. Results indicate that using an intercooler is approximately 4.5 times more effective than cooling the cooling flows directly in the turbine. It should be noted, however, that the intercooler works with lower temperature differences. In principle, therefore, the exchange area is expected to increase, causing potential cost problems and increased frontal area. In any case, it is worth taking a closer look at the use of an intercooler, possibly even changing its position in the plant layout. Losses in pressure and the efficiency of heat exchangers were not considered, limiting the benefits achievable in a real-world application. Conversely, the reduction in turbine efficiency losses related to the film cooling phenomenon was not taken into account, underestimating actual performance. Despite the long time frame, the magnitude of the improvements achievable are in line with those achieved by Lockheed-California Company for NASA-Langley Research Center in 1976-1978 [19].
Having a lower temperature flow at the exit of the high-pressure compressor could unlock the development of cycles with higher maximum temperatures and compression ratios for high specific thrust applications.
Numerous possible future developments exist in this research domain. While gas turbine technology is extensively proven, the potential uses and technological challenges associated with liquid hydrogen require in-depth technical and economic feasibility studies. Fuel storage and combustion process management, especially at high altitudes, were not extensively explored in the context of this work but still represent significant obstacles to the development of hydrogen-powered aircraft.

Contents

Nomenclature

β_i	Pressure ratio of the compressor / turbine "i"
$\dot{m}$	Mass flow rate
$\dot{V}$	Volumetric flow rate
η	Efficiency
γ	Specific heat ratio
π_d	Stagnation pressure ratio
ρ	Density
A	Area
a	Speed of sound
C_D	Drag coefficient
C_L	Lift coefficient
C_p	Specific heat
C_{D0}	Zero-lift drag coefficient
h	Enthalpy
h	Heat transfer coefficient
H_2	Hydrogen
h_T	Stagnation enthalpy
is	isentropic
k	Lift-induced drag coefficient factor
LH_2	Liquid Hydrogen
m	Mass
M_{crit}	Critical Mach number
M_{dd}	Drag divergence Mach number
MM	Molar mass
P	Pressure
P_T	Stagnation pressure
q	Dynamic pressure
R	Universal gas constant
s	Entropy
T	Temperature
T_T	Stagnation temperature
v	Flow speed
AR	Aspect Ratio
BPR	Bypass ratio
CFD	Computational Fluyd Dynamics
D	Drag force
EGT	Exhaust Gas Temperature

GE	General Electric Company
HP	High pressure
HPC	High pressure compressor
HPT	High pressure turbine
HX	Heat exchanger
ISA	International Standard Atmosphere
L	Lift force
LHV	Lower heating value
LP	Low pressure
LPT	Low pressure turbine
M	Mach number
OEW	Operating empty weight
RPM	Revolutions per minute
RPS	Revolutions per second
SFC	Specific fuel consumption
TBC	Thermal barrier coating
TIT	Turbine inlet temperature
TSEC	Thrust specific energy consumption
TSFC	Thrust specific fuel consumption
VGV	Variable guide vane

References

[1] IEA (2023), Tracking Clean Energy Progress 2023, IEA, Paris https://www.iea.org/reports/tracking-clean-energy-progress-2023, License: CC BY 4.0.

[2] Airbus, Airbus and CFM international to pioneer hydrogen combustion technology, 2022, https://www.airbus.com/en/newsroom/press-releases/2022-02-airbus-and-cfm-international-to-pioneer-hydrogen-combustion. (Accessed 07 November 2023).

[3] Airbus, Airbus reveals new zero-emission concept aircraft, 2020, article available at the following URL: https://www.airbus.com/en/newsroom/press-releases/2020-09-airbus-reveals-new-zero-emission-concept-aircraft. (Accessed 07 November 2023).

[4] Pratt Whitney, Pratt Whitney awarded department of energy project to develop hydrogen propulsion technology, 2022, https://www.prattwhitney.com/en/newsroom/news/2022/02/21/pw-awarded-department-of-energy-project-to-develop-hydrogen-propulsion-technology. (Accessed 07 November 2023).

[5] GasTurb 14 user manual | GasTurb Gmbh | RWTH Aachen University, Aachen 52062.

[6] ASTM D1655-19a, Standard Specification for Aviation Turbine Fuels. ASTM International, 2019. West Conshohocken, PA: ASTM. https://www.astm.org/Standards/D1655.htm.

[7] ExxonMobil website - Aviation fuels section, ExxonMobil.

[8] "A380 superjumbo lands in Sydney." BBC, 25 ottobre 2007.

[9] "747." | The Boeing Company website.

[10] Chiesa, Paolo. Full professor full time at Politecnico di Milano - Energy department | Verbal discussion with thesis supervisor. November 2023.

[11] CF6-80C2 series specifications. *Aircraft Commerce*, issue n. 48, 2006. Aircraft Owner's Operator's Guide.

[12] Knut Aasen, Bent Vigeland, Truls Norby, Yngve Larring, and Thor Mejdell. - development of a hydrogen membrane reformer based co2 emission free gas fired power plant. In E.S. Rubin, D.W. Keith, C.F. Gilboy, M. Wilson, T. Morris, J. Gale, and K. Thambimuthu, editors, *Greenhouse Gas Control Technologies 7*, pages 83–91. Elsevier Science Ltd, Oxford, 2005.

[13] Eytan J. Adler and Joaquim R.R.A. Martins. Hydrogen-powered aircraft: Fundamental concepts, key technologies, and environmental impacts. *Progress in Aerospace Sciences*, 141:100922, 2023. Special Issue on Green Aviation.

[14] GE Aerospace. CF680C2 engine review.

[15] GE Aerospace. CF680C2B FADEC line maintenance course. 2004. Customer Training Services, Cincinnati, Ohio 45246.

[16] P.W. Atkins and L. Jones. *Principi di chimica.* Zanichelli, 2012.

[17] Several authors and contributors. Performance prediction and simulation of gas turbine engine operation for aircraft, marine, vehicular, and power generation. *Technical report, NATO Research and Technology Organization*, 2007.

[18] Giorgio Besagni, Riccardo Mereu, Paolo Chiesa, and Fabio Inzoli. An integrated lumped parameter-cfd approach for off-design ejector performance evaluation. *Energy Conversion and Management*, 105:697–715, 2015.

[19] G D Brewer, R E Morris, G W Davis, E F Versaw, and G R Cunnington, Jr. Study of fuel systems for lh2-fueled subsonic transport aircraftvolume 2. final report, september 1976–december 1977. 7 1978.

[20] G.D. Brewer. *Hydrogen Aircraft Technology.* Taylor & Francis, 1991.

[21] Paolo Chiesa, Giovanni Gustavo Lozza, and Luigi Mazzocchi. Using hydrogen as gas turbine fuel. *Journal of Engineering for Gas Turbines and Power-transactions of The Asme*, 127:73–80, 2003.

[22] Paolo Chiesa and Ennio Macchi. A thermodynamic analysis of different options to break 60 *Journal of Engineering for Gas Turbines and Power-transactions of The Asme - J ENG GAS TURB POWER-T ASME*, 126, 10 2004.

[23] NCE Maritime CleanTech. Norwegian future value chains for liquid hydrogen. *Report. URL: https://maritimecleantech. no/wp-content/uploads/2016/11/Report-liquid-hydrogen. pdf*, 2019.

[24] Chevron Products Company. Aviation fuels. Technical review.

[25] General Electric company. Type-certficate datasheet. 2004. U.S. Department of Transportation Federal Aviation Administration, Cincinnati, Ohio 45246.

[26] General Electric company. Type-certficate datasheet. 2022. European Union Aviation Safety Agency (EASA), Cincinnati, Ohio 45246.

[27] FedEx. Presentation for training purposes of CF680C2 maintenance for A300.

[28] Antonio Filippone. Comprehensive analysis of transport aircraft flight performance. *Progress in Aerospace Sciences*, 44(3):192–236, 2008.

[29] T. H. Frost. Practical bypass mixing systems for fan jet aero engines. *Aeronautical Quarterly*, 17(2):141–160, 1966.

[30] Ohad Gur, William H. Mason, and Joseph A. Schetz. Full configuration drag estimation. *Journal of Aircraft*, 47:1356–1367, 2009.

[31] P.G. Hill and C.R. Peterson. *Mechanics and Thermodynamics of Propulsion.* Addison-Wesley, 2009.

[32] S.F. Hoerner. *Fluid-dynamic Drag: Practical Information on Aerodynamic Drag and Hydrodynamic Resistance.* Hoerner Fluid Dynamics, 1965.

[33] L.R. Jenkinson, D. Rhodes, and P. Simpkin. *Civil Jet Aircraft Design.* AIAA education series. American Insitute of Aeronautics and Astronautics, 1999.

[34] C Koroneos, A Dompros, G Roumbas, and N Moussiopoulos. Life cycle assessment of hydrogen fuel production processes. *International Journal of Hydrogen Energy*, 29(14):1443–1450, 2004.

[35] Yıldız Koç, Hüseyin Yağlı, Adnan Görgülü, and Ali Koç. Analysing the performance, fuel cost and emission parameters of the 50 mw simple and recuperative gas turbine cycles using natural gas and hydrogen as fuel. *International Journal of Hydrogen Energy*, 45(41):22138–22147, 2020.

[36] J. Kurzke and I. Halliwell. *Propulsion and Power: An Exploration of Gas Turbine Performance Modeling.* Springer International Publishing, 2018.

[37] Robert J. Le Roy, Steven G. Chapman, and Frederick R. W. McCourt. Accurate thermodynamic properties of the six isotopomers of diatomic hydrogen. *The Journal of Physical Chemistry*, 94(2):923–929, 1990.

[38] E. W. Lemmon, I. H. Bell, M. L. Huber, and M. O. McLinden. NIST Standard Reference Database 23: Reference Fluid Thermodynamic and Transport Properties-REFPROP, Version 10.0, National Institute of Standards and Technology, 2018.

[39] J.D. Mattingly, K.M. Boyer, and H. von Ohain. *Elements of Propulsion: Gas Turbines and Rockets.* AIAA education series. American Institute of Aeronautics and Astronautics, Incorporated, 2016.

[40] Bonnie McBride, Michael Zehe, and Sanford Gordon. Nasa glenn coefficients for calculating thermodynamic properties of individual species. 10 2002.

[41] Microsoft Corporation. Microsoft excel.

[42] Gordon C. Oates. Performance estimation for turbofans with and without mixers. *Journal of Propulsion and Power*, 1(3), 1985.

[43] PoliMi Department of Energy and Laboratorio Energia e Ambiente Piacenza (LEAP). Gas Steam Cycle Simulation Code - User Manual. 2016. Release 3.16.

[44] H. Pearson. Mixing of exhaust and by-pass flow in a by-pass engine. *The Aeronautical Journal*, 66(620):528–530, 1962.

[45] J. Roskam and C.T.E. Lan. *Airplane Aerodynamics and Performance*. Airplane design and analysis. Roskam Aviation and Engineering, 1997.

[46] United States Securities and Exchange Commission (SEC). Delta Airlines, Inc. Annual Reports on Form 10-K for the last 10 years.

[47] United States Securities and Exchange Commission (SEC). United Airlines Holdings, Inc. and Subsidiary Companies United Airlines, Inc. and Subsidiary Companies Annual Reports on Form 10-K for the last 10 years.

[48] Junzi Sun, Jacco Hoekstra, and Joost Ellerbroek. Aircraft drag polar estimation based on a stochastic hierarchical model. 2018.

[49] Onder Turan and Hakan Aydin. Exergetic and exergo-economic analyses of an aero-derivative gas turbine engine. *Energy*, 74:638–650, 2014.

[50] P.P. Walsh and P. Fletcher. *Gas Turbine Performance*. Wiley, 2004.

[51] PoliMi Energy Conversion Systems Group (GECOS) website software development unit. Gas Steam (GS) tool description.

[52] A Westenberger. Liquid hydrogen fuelled aircraft—system analysis, cryoplane. *European Commission, Final Report No. GRD1-1999-10014. https://cordis. europa. eu/project/id/G4RD-CT-2000-00192*, 2003.

[53] Mustagime Yildirim and Bülent Kurt. Aircraft gas turbine engine health monitoring system by real flight data. *International Journal of Aerospace Engineering*, 2018:1–12, 03 2018.

A. Elements of propulsion

The aim of this section is to revisit fundamental principles of propulsion. In particular, we will introduce and discuss the key performance indicators used to assess the performance of aircraft engines, as they will be extensively referenced throughout the document.
First, we will derive the thrust equation, and subsequently, we will introduce efficiencies and key performance parameters designed to evaluate the cost of the required thrust depending mainly on the engine design and operating conditions. These considerations take into account the cost of the energy source used and the efficiency of transforming available power into propulsive power.

A.1. Thrust

The fundamental parameter in aerospace propulsion is thrust, which is the force generated by the engine as it provides energy and accelerates the working fluid.
A general equation for thrust of air-breathing jet engines can be derived from the momentum and energy laws without the need for detailed consideration of the internal mechanisms of particular engines. In air-breathing engines, thrust is generated by increasing the momentum of the ingested and processed air. It is evident that in this case, the role of flight speed cannot be overlooked.
An additional effect of flight speed-the drag on the external surface of the engine nacelle or pod-is of secondary importance in this discussion, so for simplicity we will assume that the flow external to the engine is reversible.
Let's consider a jet engine on a test stand (Fig. 5.4), placed in a wind tunnel in such a way that it is exposed to an airstream with a velocity of u, simulating flight conditions. The control volume V and the control surface S are as indicated in the figure. The reaction to the thrust R transmitted through the structural support is indicated in figure 17.

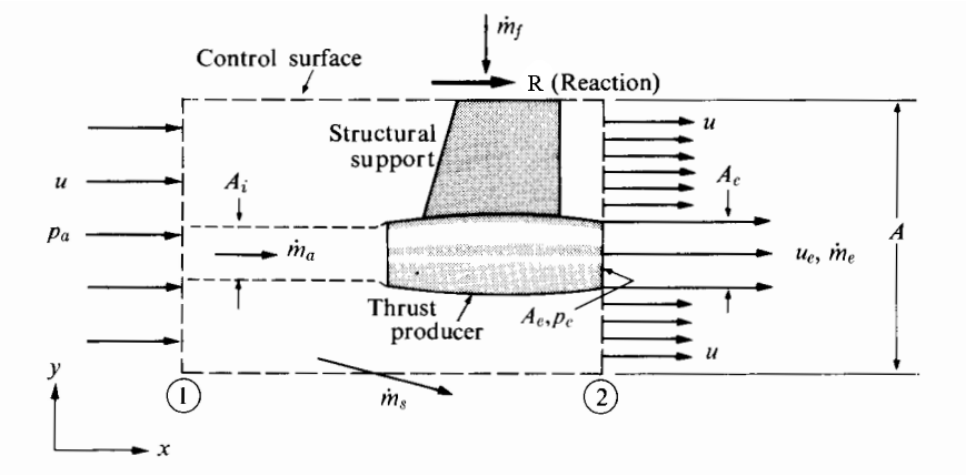

Figure 17: Generalized thrust-producing device[peters]

For the considered control volume, the principles of mass conservation (A.1) and momentum conservation (A.2) for a generic non-stationary system apply:

$$\frac{d}{dt}\int_V \rho\, dV + \int_S \rho \mathbf{u}\cdot\mathbf{n}\, dS = 0 \tag{A.1}$$

$$\sum \mathbf{F} = \frac{d}{dt}\int_V \rho \mathbf{u}\, dV + \int_S \rho \mathbf{u}(\mathbf{u}\cdot\mathbf{n})\, dS \tag{A.2}$$

Concerning mass conservation, it is observed that the engine ingests a mass flow rate of air, denoted as $\dot{m}_a$, and a mass flow rate of fuel, denoted as $\dot{m}_f$. After appropriate processing, these flows are expelled through the nozzle. Under steady-state conditions, the flow expelled through the nozzle is, therefore:

$$\dot{m}_e = \dot{m}_a + \dot{m}_f \tag{A.3}$$

Within the control volume, air mass flow $\dot{m}_{in}$ enters through the left portion of the control surface A_{in} lying in the yz plane. It exits through the side surfaces A_s of the volume with a mass flow rate $\dot{m}_s$ (in general, $\dot{m}_s$ can be positive or negative; here, it is assumed as positive when exiting), and also through the right side surface

A_{out} with a mass flow rate $\dot{m}_{out}$. A portion of the inflow from the left section passes through the engine, and similarly, the outflow from the right section includes the mass that has passed through the engine. The fuel mass flow $\dot{m}_f$ should also be considered as part of the inflow into the control volume. Thus, the mass balance is expressed as:

$$\dot{m}_{in} + \dot{m}_f = \dot{m}_s + \dot{m}_{out} \tag{A.4}$$

By combining the two expressions obtained, the mass balance for the air surrounding the engine:

$$\dot{m}_{in,ext} = \dot{m}_s + \dot{m}_{out,ext} \tag{A.5}$$

where $\dot{m}_{in,ext}$ and $\dot{m}_{out,ext}$ are defined as follows:

$$\dot{m}_{in,ext} = \dot{m}_{in} - \dot{m}_a \tag{A.6}$$

$$\dot{m}_{out,ext} = \dot{m}_{out} - \dot{m}_e \tag{A.7}$$

Regarding the conservation of momentum, the resultant of forces acting on the control volume must equal the change in the momentum flux through it. With the assumption of steady-state flow and considering the components of force and momentum flux in the x-direction only, (A.2) becomes:

$$\sum F_x = \int_S \rho u_x (\mathbf{u} \cdot \mathbf{n})\, dS \tag{A.8}$$

The forces acting on the control volume consist of the reaction force, R, necessary to keep the engine stationary, which is equal to the thrust force, T, as well as the pressure forces acting along the control surface. Air enters from the surface A_{in} with a velocity u perpendicular to the surface itself and a pressure of p_a. On the lateral surface A_s, the conditions of the air flow are those of ambient pressure and a velocity of u parallel to the considered surface (except for a small component perpendicular to allow the introduction or expulsion of mass into the control volume). From the surface A_{out}, the flow is expelled. Regarding this last surface, over most of it (precisely, $A_{out} - A_e$), the flow conditions can still be considered equal to those of the external air (u perpendicular to the surface, and $p = p_a$), while for the part related to the outlet section from the engine S_e, the conditions are indicated as p_e and u_e, with the velocity still perpendicular to the control surface.

$$\sum F_x = R + \int_{A_{in}+A_s+(A_{out}-A_e)} p_a(-\mathbf{n} \cdot \mathbf{i})\, dS + \int_{A_e} p_e(-\mathbf{n} \cdot \mathbf{i})\, dS$$

Simplifications of [Eq. sopra] is possible by observing, first of all, that the pressure forces acting along A_s are applied in a direction normal to the thrust, which results in no contribution ($\mathbf{u} \cdot \mathbf{n} = 0$). Secondly, the integral over $A_{in} + A_{out}$, regarding the first term, is zero since the two surfaces are equal for the selected control volume, and the pressure forces act in opposite directions. We have:

$$\sum F_x = R - \int_{A_e} (p_e - p_a)(\mathbf{n} \cdot \mathbf{i})\, dS = R - (p_e - p_a)A_e$$

Where the last equality is obtained by noting that on this surface $\mathbf{n} \equiv \mathbf{i}$, and the pressure p is uniform and equal to p_e at the exit section, assuming a quasi-one-dimensional flow.
As for the momentum variation (the second term of [Eq. sopra]), let's examine the flow of momentum through the control surface, decomposing it into the sections A_{in}, A_s, and A_{out}. It can be expressed as follows:

$$\int_S \rho u_x (\mathbf{u} \cdot \mathbf{n})\, dS = \int_{A_{in}} \rho u_x (\mathbf{u} \cdot \mathbf{n})\, dS + \int_{A_s} \rho u_x (\mathbf{u} \cdot \mathbf{n})\, dS + \int_{A_{out}} \rho u_x (\mathbf{u} \cdot \mathbf{n})\, dS$$

Regarding the second term on the right-hand side of [Eq. sopra], it's important to remember that in the approximation where $\mathbf{u}$ is directed as $\mathbf{i}$, there should be no mass or momentum flow through A_s. However, from [Eq. mass cons external flow], it has emerged that there is actually a mass flow (positive if outgoing), indicated as $\dot{m}_s$. The flow exiting the control volume will also carry away the corresponding momentum of the stream. It can be approximated as in [Eq. 2 qua sotto]. The three terms are:

$$\int_{A_{in}} \rho u_x (\mathbf{u} \cdot \mathbf{n})\, dS = \rho u(-u)A_{in} = -\dot{m}_{in} u$$

$$\int_{A_s} \rho u_x (\mathbf{u} \cdot \mathbf{n})\, dS \cong \dot{m}_s u$$

$$\int_{A_{out}} \rho u_x(\mathbf{u}\cdot\mathbf{n})\,dS = \int_{A_{out}-A_e} \rho u_x(\mathbf{u}\cdot\mathbf{n})\,dS + \int_{A_e} \rho u_x(\mathbf{u}\cdot\mathbf{n})\,dS = \dot{m}_{out,ext}u + \dot{m}_e u_e$$

Reformulating [Eq. completa] and substituting the results obtained in [Eq. sommaFx]:

$$R - (p_e - p_a)A_e = \dot{m}_e u_e + (\dot{m}_{out,ext} + \dot{m}_s - \dot{m}_{in})u$$

and rewriting $\dot{m}_{out,ext} + \dot{m}_s - \dot{m}_{in}$ as:

$$\dot{m}_{out,ext} + \dot{m}_s - \dot{m}_{in} = \dot{m}_{in,ext} - \dot{m}_{in} = \dot{m}_a$$

Finally, recalling that the reaction R is equal to the engine thrust T, a simple equation that describes thrust is:

$$T = (\dot{m}_a + \dot{m}_f)u_e - \dot{m}_a u + (p_e - p_a)A_e$$

The expression obtained in this way is also called "uninstalled thrust", and it represents the thrust actually generated by the engine when the only external force acting on it is the ambient pressure (which is constant). In actual flight conditions, it is necessary to consider the interaction between the aircraft and the surrounding airflow, which means that some of the assumptions, such as constant pressure on A_{in}, A_s, and especially on $A_{out} - A_e$, are no longer valid. Therefore, the thrust produced when the engine is installed on the aircraft is actually lower than the theoretical thrust obtained in [Eq. sopra] because of the installation drag. One could consider the impact of aerodynamic friction on the strut and the external surface of the engine nacelle as part of the overall aircraft drag. This factor was considered when assessing the drag in [Section x].
By separating the installation drag, which depends on the external design of the engine and its interaction with the aircraft body, the uninstalled thrust can be considered an intrinsic characteristic of the jet engine. The terms related to external forces that depend on flight velocity are included in the aerodynamic forces because they are influenced by the external shape of the engine. Therefore, when studying the engine's characteristics from now on, we will refer to the term "thrust," always implying the uninstalled thrust.
Looking at [Eq. finale], a first term, proportional to the mass flow rate expelled by the nozzle and the exhaust velocity, is known as jet thrust. The second term is negative and equal to the product of the air mass flow introduced through the intake and the airspeed, referred to as ram drag. Finally, the third term is equal to the product of the exhaust nozzle area and the difference between exhaust pressure and ambient pressure, termed pressure thrust. The pressure thrust is not zero only if the nozzle does not expand the exhaust jet to ambient pressure. This situation is only possible in the case of supersonic or sonic exhaust jets. However, it can represent a significant contribution to the thrust if the ambient pressure p_a is much less than the exhaust pressure p_e.
In the case of engines featuring two distinct exhaust streams, such as turbofan, it is necessary to apply [Eq. qdm trasformata] independently to each of these streams, differentiating between the hot (subscript H) and the cold stream (subscript C). The thrust equation for such engines takes the following form:

$$T = (\dot{m}_{aH} + \dot{m}_f)u_{eH} - \dot{m}_{aH}u + \dot{m}_{aC}(u_{eC} - u) + (p_{eH} - p_a)A_{eH} + (p_{eC} - p_a)A_{eC}$$

A.2. Propulsive Efficiency

Propulsive efficiency η_p is defined as the ratio of the useful propulsive power, which is the product of thrust and flight velocity, to the rate of production of propellant kinetic energy. For a single exhaust stream:

$$\eta_p = \frac{Tu}{\dot{m}_a((1+f)\frac{u_e^2}{2} - \frac{u^2}{2})}$$

where:

$$f = \frac{\dot{m}_f}{\dot{m}_a}$$

We can considerably simplify this expression in order to clarify its physical meaning making two reasonable assumptions. First, for modern gas turbines $f \ll 1$, so we can ignore this term in [Eq. sopra] without introducing significant errors. Second, the pressure thrust is usually much smaller than the other terms in [Eq. spinta]. Similarly, if the nozzle is fully expanded to ambient conditions, the pressure thrust is null. The equation become:

$$\eta_p \approx \frac{(u_e - u)u}{\frac{u_e^2}{2} - \frac{u^2}{2}} = \frac{2\frac{u}{u_e}}{1 + \frac{u}{u_e}}$$

The maximum value is reached for $\frac{u}{u_e} = 1$. However, in this condition the thrust is practically zero. Hence, attempting to maximize the propulsion efficiency of a jet engine is not realistic, and other parameters are necessary to evaluate its overall performance.

A.3. Thermal efficiency

Thermal efficiency ηth is defined as increase of the kinetic energy of the gas stream passing through the engine by the amount of heat employed which is given as product of fuel mass flow $\dot{m}_f$ and fuel heating value LHV_f. Again, for a single exhaust stream:

$$\eta_{th} = \frac{\dot{m}_a((1+f)\frac{u_e^2}{2} - \frac{u^2}{2})}{\dot{m}_f LHV_f}$$

A.4. Overall efficiency

The product $eta_p eta_{th}$, is called the overall efficiency, eta_o , and is defined by:

$$\eta_o = \frac{Tu}{\dot{m}_f LHV_f}$$

and with the assumption of $f \ll 1$:

$$\eta_o = 2\eta_{th}\left(\frac{\frac{u}{u_e}}{1+\frac{u}{u_e}}\right)$$

The significance of overall efficiency will become clearer in the next section.

A.5. Specific Fuel Consumption

One of the most critical parameters in measuring the performance of an engine is specific fuel consumption SFC, which indicates the amount of fuel required per unit of time to achieve a reference performance. Since its value greatly depends on the flight conditions, static conditions are often used as a common reference point. Specifically, for jet engines, the reference is the thrust generated by the engine, hence the acronym $TSFC$. Its expression is:

$$TSFC = \frac{\dot{m}_f}{T}$$

Note that the $TSFC$, by multiplying both the numerator and denominator in its definition by $uLHV_f$, can be expressed as follows:

$$TSFC = \frac{1}{\eta_o}\frac{u}{LHV_f}$$

Therefore, it is essentially, given the flight velocity u, inversely proportional to overall efficiency. It is, therefore, useful for comparing the performance of propulsion systems that power aircraft flying at nearly the same speed, such as modern commercial jetliners, even with different rated thrust. Although fuel consumption has no direct effect on performance, the fuel flow has a great influence on the operational costs of an aircraft.

B. GasTurb off-design simulation

To predict component efficiencies at conditions differing from the cycle reference point, it is essential to have suitable component maps. Since genuine component maps may not be accessible, substitutes must be generated during the model creation process. Obtaining realistic maps is essential for high-quality gas turbine performance calculations. While direct map generation is mainly feasible for engine manufacturers, GasTurb users must adapt existing maps from the literature to align with available data.
For the off-design model, it's crucial to establish a strong match between the given data and the simulation at the cycle reference point, as the model is finely tuned during the cycle design phase. The cycle reference point serves as the foundation for all off-design modeling work, and it remains unaltered after the tuning process is completed. In this regard, the first step involved replicating, as accurately as possible, the same conditions for the takeoff simulation. This procedure not only established a starting point for the off-design calculations but also facilitated the comparison of results obtained using two different software platforms. This also served as an additional validation check for the GS cycle resolution algorithm.
When constructing the off-design model starting with standard maps, it's highly recommended to select standard maps of components similar to those of the engine being simulated in terms of flow path (axial or centrifugal), operating regime (subsonic, transonic, supersonic), number of stages and other relevant parameters [36]. These design choices can significantly impact the map's shape. For instance, in axial compressors, the pressure ratio and map shape are correlated, making it important to match the map with the engine's design pressure ratios. Concerning the flow regime, supersonic velocities can exist in the flow relative to the rotor of the first compressor stage. In such a case, the lines for higher corrected blade speed are vertical over a wide range of pressure ratios because the flow field upstream of the first rotor does not change. The map of a single stage fan is an example in which supersonic flow in the rotor is the reason for the speed lines being vertical in the high-speed region. Conversely, the boosters of ungeared turbofan engines, which operate at low circumferential speeds, do not experience supersonic flow at their entry, resulting in a completely different behavior. In addition, if the general level of Mach number in a compressor is high, the efficiency islands in the corresponding map are narrower than in those where Mach numbers are more moderate. Therefore, selecting appropriate standard maps tailored to the specific case of study is essential to establish a solid foundation and avoid significant errors.

GasTurb scales the maps automatically in such a way that the calculation of the cycle design point in the off-design simulation mode agrees with the results of the cycle design calculation in every detail [5]. Calculation and assumptions regarding the cycle design point has yielded values for pressure ratios, polytropic/isentropic efficiencies and corrected flows. Since the combination of these three numbers will not be found in the standard map available the question arises: "Where in the unscaled map is the map scaling point corresponding to the cycle design point?"
When Standard Maps are selected in GasTurb, the program locates the scaling point using preset map coordinates. However, it's clear that the default selection of the map scaling point may not be universally accurate for all engines. The correct positioning of this point depends on the location of the cycle design point within the engine's operating envelope (takeoff, cruise condition, climb, landing etc.). Attention must be paid to this manual selection, because it has implications on the speed values, the general level of efficiency, the maximum corrected flow and obviously on the resulting off-design pressure ratio.

When dealing with compressors, there are some general guidelines to consider. If the cycle design point corresponds to cruising conditions, it is advisable to position the scaling point within the peak efficiency region of the map based on the manufacturer's design choice [39]. On the other hand, if the design conditions relate to takeoff, the compressor's operating line will be likely to be out the maximum efficiency region [36]
When it comes to turbines, their aerodynamic design is primarily aimed at achieving minimal losses during their cruise operation. As it will be explained, turbines operate most of the time at the pressure ratio for which they were designed. This is because these turbines operate within a very narrow range. Hence, the turbine map does not significantly impact the quality of the simulation.
Next, the discussion will delve into how these points were established in the various maps, taking into account the overall physical behavior of the system and the operation of individual components.

Fan The bypass nozzle dominates the fan operating line of a turbofan with separate cold and hot nozzles. The corrected flow through the bypass nozzle depends on the pressure ratio accross the nozzle and that has an inverse relationship to the bypass ratio. The corrected flow per unit area through a nozzle reaches its maximum at sonic conditions, where $M = 1$. Note that for a given area the corrected flow reaches 90% of its maximum value when Mach number is only 0.68, as shown in Fig. sotto. Thus, theoretical considerations based on the assumption of sonic flow are useful also for high subsonic Mach number.

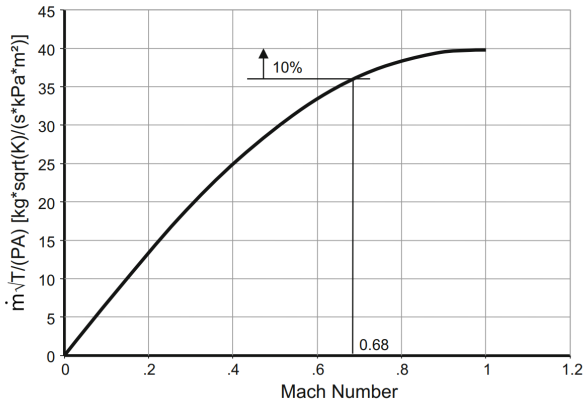

Figure 18: Reduced flow per area through a nozzle [36]

During cruise the bypass nozzle pressure ratio is above the critical value, i.e. the flow is sonic even for very high bypass ratio engines. At take off conditions, the nozzle pressure ratio becomes typically sub-critical and the corrected fan exit flow gets smaller. This difference in pressure ratios can be mainly attributable to the ram effect at high flight speeds. However, the bypass nozzle Mach number at sea level static take off is $M = 0.9$, the corrected flow is only slightly less than at cruise. As a result the cruise point in the fan map should be very near to the take off point. The considerations change when dealing with particularly high bypass ratios, like in the most modern turbofan engines. In such cases, the fan typically exhibits a lower compression ratio. As a result, the nozzle pressure ratio will be significantly lower than the critical one at take off, making this assumption no longer valid.

HPC The choice of the standard HPC map was driven by opting for an axial configuration and selecting a range of compression ratios that contained the one used in the takeoff simulation. The scaling point was selected to ensure that under cruise conditions, the operating point falls within the region of maximum efficiency. No further adjustments were deemed necessary.

Booster The operating point of a turbofan's booster is influenced by both the downstream high-pressure compressor (HPC) and the fan, as they share the same spool speed. In an ungeared turbofan, the booster is constrained to rotate at a speed equal to that of the fan, typically resulting in low circumferential speeds. Consequently, the airflow is generally subsonic. For simulating an ungeared turbofan with a bypass ratio of 5, the GasTurb Standard booster map is not a suitable choice. Conversely, it is well-suited for simulating the booster of a turbofan equipped with a gearbox, where these compressors operate at higher circumferential speeds and Mach numbers. To address this issue, a subsonic compressor was manually selected. The considerations for the subsequent placement of the scaling point are the same as those made for the HPC.

HPT The pressure ratio of the CF6-80C2 HPT remains constant, as is the case with any gas generator turbine. The corrected speed experiences only minor variations. The operating line is notably short and that is why reading the HPT map nearly always yields the same efficiency. Consequently, the shape of the efficiency islands in the map has minimal influence on simulation accuracy. Alterations to turbine efficiency originate primarily from changes in running tip clearance, not from locating the operating point incorrectly in the map. A big error cannot be made if the map scaling point is set somewhere in the middle of the high efficiency area. Using the GasTurb Standard map in combination with the default coordinates of the map scaling point is deemed suitable for this case.

LPT The LPT pressure ratio remains constant as long as the core nozzle is choked. The considerations are almost valid also for subsonic flows given the trend of the reduced flow per unit area depicted in Fig. 18. It should be noted, however, that for core nozzle the intake is less rigorous than for the nozzle bypass. As mentioned for the fan, this is particularly applicable in the higher thrust range of low bypass ratio turbofans. With increasing bypass ratios, the fan's design pressure ratio decreases, consequently reducing the velocity of the bypass jet. The core jet velocity closely follows the bypass jet velocity, as the optimal ratio between them remains relatively stable in well-designed engines. Under these assumptions, the same tuning procedure adopted for the HPT is also applicable for the LPT. Although the operating line is longer compared to that of the HPT, it still does not warrant significant efficiency alterations.

The variation in the total pressure ratio has been considered in accordance with section 2.1, while the combustor and nozzle performance has not been changed.

C. Tables of thermodynamic properties

The following tables are reported to provide more clarity on the individual thermodynamic stations. All reported temperature and pressure values are intended as stagnation variables.

Table 6: Thermodynamic stations - Jetfuel - Takeoff phase

Flow number	Temperature [°C]	Pressure [bar]	Mass flow [kg/s]	Molar flow [kmol/s]
1	15.0	1.01	790.00	27.28
2	15.0	1.00	790.00	27.28
3	67.5	1.71	790.00	27.28
4	67.5	1.71	128.45	4.43
5	178.9	4.20	128.45	4.43
6	178.9	4.20	123.47	4.26
7	550.2	30.00	123.47	4.26
8	550.2	30.00	120.29	4.15
9	1250.3	29.39	122.81	4.24
10	894.9	8.78	130.97	4.52
11	527.5	1.62	130.97	4.52
12	527.5	1.61	130.97	4.52
13	67.5	1.71	661.52	22.84
14	67.5	1.69	661.52	22.84
15	178.9	4.20	4.98	0.17
16	550.2	30.00	3.19	0.11
17	15.0	50.00	2.52	0.18

Table 7: Molar fractions - Jetfuel - Takeoff phase

Flow number	Molar fraction [%]										
	Ar	N2	O2	H2	C2H6	C	H2S	CO	CO2	H2O	SO2
1	0.930	78.090	20.950	0.000	0.000	0.000	0.000	0.000	0.030	0.000	0.000
2	0.930	78.090	20.950	0.000	0.000	0.000	0.000	0.000	0.030	0.000	0.000
3	0.930	78.090	20.950	0.000	0.000	0.000	0.000	0.000	0.030	0.000	0.000
4	0.930	78.090	20.950	0.000	0.000	0.000	0.000	0.000	0.030	0.000	0.000
5	0.930	78.090	20.950	0.000	0.000	0.000	0.000	0.000	0.030	0.000	0.000
6	0.930	78.090	20.950	0.000	0.000	0.000	0.000	0.000	0.030	0.000	0.000
7	0.930	78.090	20.950	0.000	0.000	0.000	0.000	0.000	0.030	0.000	0.000
8	0.930	78.090	20.950	0.000	0.000	0.000	0.000	0.000	0.030	0.000	0.000
9	0.911	76.535	14.334	0.000	0.000	0.000	0.000	0.000	4.270	3.947	0.003
10	0.913	76.632	14.747	0.000	0.000	0.000	0.000	0.000	4.005	3.701	0.003
11	0.913	76.632	14.747	0.000	0.000	0.000	0.000	0.000	4.005	3.701	0.003
12	0.913	76.632	14.747	0.000	0.000	0.000	0.000	0.000	4.005	3.701	0.003
13	0.930	78.090	20.950	0.000	0.000	0.000	0.000	0.000	0.030	0.000	0.000
14	0.930	78.090	20.950	0.000	0.000	0.000	0.000	0.000	0.030	0.000	0.000
15	0.930	78.090	20.950	0.000	0.000	0.000	0.000	0.000	0.030	0.000	0.000
16	0.930	78.090	20.950	0.000	0.000	0.000	0.000	0.000	0.030	0.000	0.000
17	0.000	0.000	0.000	23.846	22.677	52.567	0.064	0.845	0.000	0.000	0.000

Table 8: Thermodynamic stations - Jetfuel - Cruise phase

Flow number	Temperature [°C]	Pressure [bar]	Mass flow [kg/s]	Molar flow [kmol/s]
1	-25.9	0.37	238.62	8.24
2	-25.9	0.37	238.62	8.24
3	19.2	0.62	238.62	8.24
4	19.2	0.62	38.80	1.34
5	41.9	0.79	38.80	1.34
6	41.9	0.79	37.36	1.29
7	399.3	8.87	37.36	1.29
8	399.3	8.87	36.46	1.26
9	1173.6	8.70	37.28	1.29
10	835.8	2.59	39.63	1.37
11	583.8	0.82	39.63	1.37
12	583.8	0.81	39.63	1.37
13	19.2	0.62	199.82	6.90
14	19.2	0.62	199.82	6.90
15	41.9	0.79	1.44	0.05
16	399.3	8.87	0.90	0.03
17	15.0	50.00	0.83	0.06

Table 9: Molar fractions - Jetfuel - Cruise phase

Flow number	Molar fraction [%]										
	Ar	N2	O2	H2	C2H6	C	H2S	CO	CO2	H2O	SO2
1	0.930	78.090	20.950	0.000	0.000	0.000	0.000	0.000	0.000	0.030	0.000
2	0.930	78.090	20.950	0.000	0.000	0.000	0.000	0.000	0.000	0.030	0.000
3	0.930	78.090	20.950	0.000	0.000	0.000	0.000	0.000	0.000	0.030	0.000
4	0.930	78.090	20.950	0.000	0.000	0.000	0.000	0.000	0.000	0.030	0.000
5	0.930	78.090	20.950	0.000	0.000	0.000	0.000	0.000	0.000	0.030	0.000
6	0.930	78.090	20.950	0.000	0.000	0.000	0.000	0.000	0.000	0.030	0.000
7	0.930	78.090	20.950	0.000	0.000	0.000	0.000	0.000	0.000	0.030	0.000
8	0.930	78.090	20.950	0.000	0.000	0.000	0.000	0.000	0.000	0.030	0.000
9	0.910	76.413	13.817	0.000	0.000	0.000	0.000	0.000	4.601	4.256	0.003
10	0.911	76.512	14.239	0.000	0.000	0.000	0.000	0.000	4.331	4.004	0.003
11	0.911	76.512	14.239	0.000	0.000	0.000	0.000	0.000	4.331	4.004	0.003
12	0.911	76.512	14.239	0.000	0.000	0.000	0.000	0.000	4.331	4.004	0.003
13	0.930	78.090	20.950	0.000	0.000	0.000	0.000	0.000	0.000	0.030	0.000
14	0.930	78.090	20.950	0.000	0.000	0.000	0.000	0.000	0.000	0.030	0.000
15	0.930	78.090	20.950	0.000	0.000	0.000	0.000	0.000	0.000	0.030	0.000
16	0.930	78.090	20.950	0.000	0.000	0.000	0.000	0.000	0.000	0.030	0.000
17	0.000	0.000	0.000	23.846	22.677	52.567	0.064	0.845	0.000	0.000	0.000

Table 10: Thermodynamic stations - Hydrogen - Takeoff phase

Flow number	Temperature [°C]	Pressure [bar]	Mass flow [kg/s]	Molar flow [kmol/s]
1	15.0	1.01	790.00	27.28
2	15.0	1.00	790.00	27.28
3	67.5	1.71	790.00	27.28
4	67.5	1.71	128.45	4.43
5	178.9	4.20	128.45	4.43
6	178.9	4.20	124.33	4.29
7	550.2	30.00	124.33	4.29
8	550.2	30.00	121.51	4.20
9	1206.1	29.39	122.39	4.41
10	865.0	8.86	129.33	4.65
11	502.6	1.63	129.33	4.65
12	502.6	1.62	129.33	4.65
13	67.5	1.71	661.52	22.84
14	67.5	1.69	661.52	22.84
15	178.9	4.20	4.12	0.14
16	550.2	30.00	2.82	0.10
17	15.0	50.00	0.88	0.44

Table 11: Molar fractions - Hydrogen - Takeoff phase

Flow number	Molar fraction [%]										
	Ar	N2	O2	H2	C2H6	C	H2S	CO	CO2	H2O	SO2
1	0.930	78.090	20.950	0.000	0.000	0.000	0.000	0.000	0.000	0.030	0.000
2	0.930	78.090	20.950	0.000	0.000	0.000	0.000	0.000	0.000	0.030	0.000
3	0.930	78.090	20.950	0.000	0.000	0.000	0.000	0.000	0.000	0.030	0.000
4	0.930	78.090	20.950	0.000	0.000	0.000	0.000	0.000	0.000	0.030	0.000
5	0.930	78.090	20.950	0.000	0.000	0.000	0.000	0.000	0.000	0.030	0.000
6	0.930	78.090	20.950	0.000	0.000	0.000	0.000	0.000	0.000	0.030	0.000
7	0.930	78.090	20.950	0.000	0.000	0.000	0.000	0.000	0.000	0.030	0.000
8	0.930	78.090	20.950	0.000	0.000	0.000	0.000	0.000	0.000	0.030	0.000
9	0.910	76.413	13.817	0.000	0.000	0.000	0.000	0.000	4.601	4.256	0.003
10	0.911	76.512	14.239	0.000	0.000	0.000	0.000	0.000	4.331	4.004	0.003
11	0.911	76.512	14.239	0.000	0.000	0.000	0.000	0.000	4.331	4.004	0.003
12	0.911	76.512	14.239	0.000	0.000	0.000	0.000	0.000	4.331	4.004	0.003
13	0.930	78.090	20.950	0.000	0.000	0.000	0.000	0.000	0.000	0.030	0.000
14	0.930	78.090	20.950	0.000	0.000	0.000	0.000	0.000	0.000	0.030	0.000
15	0.930	78.090	20.950	0.000	0.000	0.000	0.000	0.000	0.000	0.030	0.000
16	0.930	78.090	20.950	0.000	0.000	0.000	0.000	0.000	0.000	0.030	0.000
17	0.000	0.000	0.000	100.000	0.000	0.000	0.000	0.000	0.000	0.000	0.000

Table 12: Thermodynamic stations - Hydrogen, $\Delta h = 1750 kJ/kg$ - Takeoff phase

Flow number	**Temperature [°C]**	**Pressure [bar]**	**Mass flow [kg/s]**	**Molar flow [kmol/s]**
1	15	1.01	790.00	27.28
2	15	1.00	790.00	27.28
3	67.5	1.71	790.00	27.28
4	67.5	1.71	128.45	4.43
5	178.9	4.20	128.45	4.43
6	178.9	4.20	128.45	4.43
7	178.9	4.20	125.59	4.34
8	550.1	30.00	125.59	4.34
9	550.1	30.00	121.96	4.21
10	1248.3	29.39	122.89	4.44
11	900.6	9.20	129.38	4.67
12	542.2	1.82	129.38	4.67
13	542.2	1.80	129.38	4.67
14	67.5	1.71	661.52	22.84
15	67.5	1.69	661.52	22.84
16	178.9	4.20	2.86	0.10
17	550.1	29.99	3.63	0.13
18	125.4	29.99	3.63	0.13
19	15	50.00	0.93	0.46
20	136.6	50.00	0.93	0.46
21	136.6	50.00	0.93	0.46

Table 13: Molar fractions - Hydrogen, $\Delta h = 1750 kJ/kg$ - Takeoff phase

Flow number	**Molar fraction [%]**										
	Ar	**N2**	**O2**	**H2**	**C2H6**	**C**	**H2S**	**CO**	**CO2**	**H2O**	**SO2**
1	0.930	78.090	20.950	0.000	0.000	0.000	0.000	0.000	0.000	0.030	0.000
2	0.930	78.090	20.950	0.000	0.000	0.000	0.000	0.000	0.000	0.030	0.000
3	0.930	78.090	20.950	0.000	0.000	0.000	0.000	0.000	0.000	0.030	0.000
4	0.930	78.090	20.950	0.000	0.000	0.000	0.000	0.000	0.000	0.030	0.000
5	0.930	78.090	20.950	0.000	0.000	0.000	0.000	0.000	0.000	0.030	0.000
6	0.930	78.090	20.950	0.000	0.000	0.000	0.000	0.000	0.000	0.030	0.000
7	0.930	78.090	20.950	0.000	0.000	0.000	0.000	0.000	0.000	0.030	0.000
8	0.930	78.090	20.950	0.000	0.000	0.000	0.000	0.000	0.000	0.030	0.000
9	0.930	78.090	20.950	0.000	0.000	0.000	0.000	0.000	0.000	0.030	0.000
10	0.882	74.035	14.669	0.000	0.000	0.000	0.000	0.000	0.280	10.386	0.000
11	0.884	74.229	14.970	0.000	0.000	0.000	0.000	0.000	0.290	9.888	0.000
12	0.884	74.229	14.970	0.000	0.000	0.000	0.000	0.000	0.290	9.888	0.000
13	0.884	74.229	14.970	0.000	0.000	0.000	0.000	0.000	0.290	9.888	0.000
14	0.930	78.090	20.950	0.000	0.000	0.000	0.000	0.000	0.000	0.030	0.000
15	0.930	78.090	20.950	0.000	0.000	0.000	0.000	0.000	0.000	0.030	0.000
16	0.930	78.090	20.950	0.000	0.000	0.000	0.000	0.000	0.000	0.030	0.000
17	0.930	78.090	20.950	0.000	0.000	0.000	0.000	0.000	0.000	0.030	0.000
18	0.930	78.090	20.950	0.000	0.000	0.000	0.000	0.000	0.000	0.030	0.000
19	0.000	0.000	0.000	100.000	0.000	0.000	0.000	0.000	0.000	0.000	0.000
20	0.000	0.000	0.000	100.000	0.000	0.000	0.000	0.000	0.000	0.000	0.000
21	0.000	0.000	0.000	100.000	0.000	0.000	0.000	0.000	0.000	0.000	0.000

Table 14: Thermodynamic stations - Hydrogen, $\Delta h = 4500 kJ/kg$ - Takeoff phase

Flow number	**Temperature [°C]**	**Pressure [bar]**	**Mass flow [kg/s]**	**Molar flow [kmol/s]**
1	15.0	1.01	790.00	27.28
2	15.0	1.00	790.00	27.28
3	67.5	1.71	790.00	27.28
4	67.5	1.71	128.45	4.43
5	178.9	4.20	128.45	4.43
6	159.7	4.20	128.45	4.43
7	159.7	4.20	125.94	4.35
8	517.9	30.00	125.94	4.35
9	517.9	30.00	122.64	4.23
10	1222.1	29.39	123.55	4.46
11	889.0	9.53	129.36	4.66
12	529.3	1.84	129.36	4.66
13	529.3	1.82	129.36	4.66
14	67.5	1.71	661.52	22.84
15	67.5	1.69	661.52	22.84
16	159.7	4.20	2.51	0.09
17	517.9	30.00	3.30	0.11
18	55.2	30.00	3.30	0.11
19	15.0	50.00	0.91	0.45
20	136.6	50.00	0.91	0.45
21	326.1	50.00	0.91	0.45

Table 15: Molar fractions - Hydrogen, $\Delta h = 4500 kJ/kg$ - Takeoff phase

Flow number	**Molar fraction [%]**										
	Ar	**N2**	**O2**	**H2**	**C2H6**	**C**	**H2S**	**CO**	**CO2**	**H2O**	**SO2**
1	0.930	78.090	20.950	0.000	0.000	0.000	0.000	0.000	0.000	0.030	0.000
2	0.930	78.090	20.950	0.000	0.000	0.000	0.000	0.000	0.000	0.030	0.000
3	0.930	78.090	20.950	0.000	0.000	0.000	0.000	0.000	0.000	0.030	0.000
4	0.930	78.090	20.950	0.000	0.000	0.000	0.000	0.000	0.000	0.030	0.000
5	0.930	78.090	20.950	0.000	0.000	0.000	0.000	0.000	0.000	0.030	0.000
6	0.930	78.090	20.950	0.000	0.000	0.000	0.000	0.000	0.000	0.030	0.000
7	0.930	78.090	20.950	0.000	0.000	0.000	0.000	0.000	0.000	0.030	0.000
8	0.930	78.090	20.950	0.000	0.000	0.000	0.000	0.000	0.000	0.030	0.000
9	0.930	78.090	20.950	0.000	0.000	0.000	0.000	0.000	0.000	0.030	0.000
10	0.883	74.127	14.811	0.000	0.000	0.000	0.000	0.000	0.028	10.151	0.000
11	0.885	74.297	15.076	0.000	0.000	0.000	0.000	0.000	0.029	9.714	0.000
12	0.885	74.297	15.076	0.000	0.000	0.000	0.000	0.000	0.029	9.714	0.000
13	0.885	74.297	15.076	0.000	0.000	0.000	0.000	0.000	0.029	9.714	0.000
14	0.930	78.090	20.950	0.000	0.000	0.000	0.000	0.000	0.000	0.030	0.000
15	0.930	78.090	20.950	0.000	0.000	0.000	0.000	0.000	0.000	0.030	0.000
16	0.930	78.090	20.950	0.000	0.000	0.000	0.000	0.000	0.000	0.030	0.000
17	0.930	78.090	20.950	0.000	0.000	0.000	0.000	0.000	0.000	0.030	0.000
18	0.930	78.090	20.950	0.000	0.000	0.000	0.000	0.000	0.000	0.030	0.000
19	0.000	0.000	0.000	100.000	0.000	0.000	0.000	0.000	0.000	0.000	0.000
20	0.000	0.000	0.000	100.000	0.000	0.000	0.000	0.000	0.000	0.000	0.000
21	0.000	0.000	0.000	100.000	0.000	0.000	0.000	0.000	0.000	0.000	0.000

Abstract in lingua italiana

L'espansione dell'aviazione civile globale e l'importante impatto ambientale legato alle emissioni di CO_2 richiedono soluzioni innovative in linea con gli obiettivi ambientali. L'idrogeno, in sinergia con i già diffusi motori a getto, si presenta come un eccellente candidato per realizzare voli a zero emissioni di carbonio, sfruttando una tecnologia consolidata e potenziali miglioramenti delle prestazioni.
Nel contesto del progetto europeo EFACA (Environmentally Friendly Aviation for All Classes of Aircraft), questa ricerca analizza in modo approfondito un sistema di alimentazione a idrogeno liquido utilizzando un codice informatico proprietario del Politecnico di Milano. Sono stati apportati miglioramenti al software per modellare l'aspirazione dell'aria e gli ugelli a flusso separato e misto, consentendo la valutazione delle prestazioni del motore aereo. Successivamente, è stata condotta la progettazione e la simulazione di nuove soluzioni impiantistiche per sfruttare il potenziale di raffreddamento dell'idrogeno liquido, ottenendo un miglioramento del 4% nel consumo di energia specifico alla spinta durante la transizione dal carburante convenzionale jetfuel.
I risultati indicano possibili sviluppi futuri, mettendo in luce la necessità di approfondire ulteriormente i benefici di tali sistemi e, contemporaneamente, di affrontare le sfide legate a stoccaggio, combustione e produzione dell'idrogeno, che attualmente limitano la loro fattibilità tecnico-economica. Questa ricerca contribuisce agli attuali sforzi nella ricerca di soluzioni di aviazione eco-sostenibili, allineandosi con l'obiettivo di raggiungere la neutralità carbonica entro il 2050.

Parole chiave: idrogeno, simulazione, aereo, turbofan, propulsione, presa d'aria, ugello

Ringraziamenti

Questo lavoro rappresenta la pietra angolare di un percorso durato 5 anni, un percorso fatto di sfide, nuove amicizie, addii, scoperte e crescita personale.
Desidero ringraziare sinceramente tutte le persone che mi hanno accompagnato e supportato in questo viaggio, contribuendo a modo loro al raggiungimento di questo importante traguardo. A ciascuna di loro, dedico queste brevi parole di riconoscimento.

Ai miei genitori
Chiaramente senza di voi tutto questo non sarebbe stato possibile. Grazie per per aver condiviso le gioie dei successi e per esservi uniti a me durante i fallimenti. Le vostre parole di saggezza e il vostro costante sostegno hanno forgiato il mio carattere. Amore incondizionato, coraggio, integrità, resilienza, dedizione, equanimità, generosità, responsabilità e tolleranza sono solo alcuni dei valori che siete riusciti a trasmettermi, garantendo una vita migliore a me e a chi mi circonda. In ogni capitolo della mia vita avete fatto del vostro meglio. Ogni sacrificio che avete fatto, ogni notte insonne e ogni sorriso incoraggiante non sono stati vani e hanno contribuito a plasmare il successo che oggi celebriamo. Siete e sarete sempre al centro dei miei pensieri.

Ai nonni
A nonno Vincenzo e nonna Lucia, pur avendo trascorso solo pochi anni insieme, la vostra semplicità e bontà d'animo hanno lasciato un'impronta indelebile nei valori che oggi incarno. Siete stati i pilastri silenziosi ma potenti su cui si è fondata la mia famiglia, e la vostra eredità di amore e saggezza continua a guidare ogni mio passo.
A nonno Domenico e nonna Grazia, la gratitudine è un sentimento che trascende le parole. I vostri sacrifici e la vostra costante premura hanno reso la mia vita più ricca e significativa. Fareste qualsiasi cosa per la felicità dei vostri nipoti perchè è ciò che rende feliici anche voi. Ogni momento con voi è un tesoro dal valore inestimabile.

A Miriana
A lei, il mio amore e la mia roccia in questo straordinario percorso. Sei l'incarnazione stessa della purezza, dire una bugia per te sarebbe come negare la luce del sole. La tua generosità è un faro nella mia vita, e ogni giorno mi insegna il vero significato dell'amore altruista. La nostra relazione a distanza è stata una prova durevole, ma hai dimostrato una forza e una pazienza straordinarie. La tua presenza costante è l'ossigeno che ha tenuto viva la fiamma della nostra relazione, nonostante la distanza. Ogni giorno lontano è stato un passo più vicino al futuro che ora ci aspetta. Non vedo l'ora di condividere ogni momento che il futuro ci riserva con te.

A Domenico
Sebbene non dimostri sempre il tuo affetto, dopo quasi 25 anni ho capito di essere sempre e comunque l'unico fratello che potessi desiderare e che ti potesse sopportare. Ovviamente vale anche il reciproco. Ormai è chiaro che faremmo follie pur di vederci felici, ma continueremo ovviamente a far finta di niente. Grazie anche per la tua franchezza e la tua durezza quando necessario, mi ha spinto a migliorarmi e crescere.

Agli amici di sempre
Il tempo passa e tutto sembra cambiare velocemente, il nostro legame sembra invece resistere al trascorrere del tempo, mantenendo la stessa sincerità e genuinità di 10 anni fa. Questo vale ancor di più per chi, come me, è stato lontano per lunghi periodi. In questi anni, abbiamo imparato che la forza del nostro legame risiede nella capacità di stare bene insieme, indipendentemente dalle circostanze. Non serve altro, solo la gioia di condividere la vita l'uno con l'altro. Grazie per esserci sempre, rendendo ogni istante un ricordo indelebile nella nostra storia condivisa.

A Matteo
Iniziare questa dedica senza sottolineare quanto la nostra storia sia iniziata con basse aspettative sarebbe sminuire il viaggio straordinario che abbiamo compiuto insieme partendo da quell'ultimo banco. Ci siamo incontrati quando eravamo già "grandi", ma nel corso del tempo, abbiamo trasformato quelle aspettative in un legame unico. È difficile trovare le parole per esprimere quanto la tua presenza abbia arricchito la mia esperienza e quanto io sia grato di averti come cugino.

A Lorenza
Fin dall'inizio, abbiamo capito che volevamo contribuire al benessere dell'altro senza secondi fini, e nel tempo questa promessa si è trasformata in una realtà tangibile. Le risate condivise, gli incoraggiamenti e il sostegno sono diventati i pilastri su cui poggia la nostra amicizia. Con affetto, grazie per essere la persona straordinaria che sei.